ADVANCED ENERGY MATERIALS
www.advenergymat.de

Photon- and Charge-Management in Advanced Energy Materials: Combining 0D, 1D, and 2D Nanocarbons as well as Bulk Semiconductors with Organic Chromophores

*Alejandro Cadranel, Philipp Haines, Ramandeep Kaur, Arjun Menon, Peter W. Münich, Peter R. Schol, and Dirk M. Guldi**

In this contribution, seminal works in the area of photon- and charge-management are highlighted with focus on covalent electron donor-acceptor conjugates built around porphyrins (Ps), on one hand, and 0D, 1D, and 2D nanocarbons, on the other hand. Photons in these conjugates are managed by Ps, while 0D, 1D, and 2D nanocarbons serve as the active component, which enable managing charges. With a few leading examples, it can be explored much beyond the simple photon- and charge-management characterization and emphasize photovoltaics and photocatalysis to convert and store energy. This contribution concludes by highlighting recent progress in mixing and matching the unique charge-management features of nanocarbons in the design of multidimensional nanocarbons.

1. Introduction

Photosynthesis is performed by all plants, algae, and even some microorganisms and is based on the use of light energy to produce sugars from carbon dioxide and water. For photosynthesis to perform well, a sophisticated synergy of photon- and charge-management is required. Artificial photosynthesis attempts to replicate the natural processes of photosynthesis, that is, to convert sunlight, a practically unlimited and sustainable source of energy, to make high-energy chemicals to store energy.[1–3]

Nature provides the perfect blueprint for an optimized photon- and charge-management.[4–7] With focus on photon-management, it is the light-harvesting within an array of proteins, carotenoids, and chlorophylls that enables unidirectional transfer of light energy. Important is hereby that, the absorption spectra of the individual building blocks are non-overlapping. As a consequence, they broaden the range of light that is absorbed, and that sets up the ways and means to panchromaticity. In short, panchromaticity is an optical feature that ensures the absorption of light across the entire visible spectral region. In non-natural/artificial systems, panchromaticity is realized by combining two or more photoactive building blocks, each with complementary absorptions. Porphyrinoid systems—vide infra—stand out in this context as they guarantee tailoring energy gradients at ease. Currently, down- and up-conversions receive increasing interest as a versatile platform for photon-management as it enables improving energy harvesting over the whole solar spectrum. The down-conversion of singlet excited states by means of multiexciton generation/singlet fission enables multiple excitons to be generated after the absorption of just a single photon. For example, by integrating multiexciton generation/singlet fission materials into solar-cell architectures, it is feasible to overall increase the efficiency of solar cells by pushing the Shockley–Queisser limit from 32% to approximately 45%. Up-conversion is, from a fundamental perspective, the reversion of multiexciton generation/singlet fission, since multiple low-energy excitons are converted into a single high-energy photon. Yet, another approach to manage photons is based on non-linear processes such as two-photon absorptions.

When turning to charge-management, the Marcus theory of charge-transfer is considered.[8] It stands out as the dominant theory of charge-transfer in chemistry and treats its rate constants as a parabolic dependence on the free energy changes of the reaction. The underlying relationship provides a valuable guide for control over the efficiency and kinetics of charge-management

Dr. A. Cadranel, P. Haines, R. Kaur, A. Menon, Dr. P. W. Münich, P. R. Schol, Prof. D. M. Guldi
Department of Chemistry and Pharmacy
Interdisciplinary Center for Molecular Materials
Friedrich-Alexander Universität Erlangen-Nürnberg
Egerlandstraße 3, Erlangen 91058, Germany
E-mail: dirk.guldi@fau.de
Dr. A. Cadranel
Universidad de Buenos Aires
Facultad de Ciencias Exactas y Naturales
Departamento de Química Inorgánica
Analítica y Química Física
Pabellón 2, Ciudad Universitaria
Buenos Aires C1428EHA, Argentina
Dr. A. Cadranel
CONICET—Universidad de Buenos Aires
Instituto de Química-Física de Materiales
Medio Ambiente y Energía (INQUIMAE)
Pabellón 2, Ciudad Universitaria
Buenos Aires C1428EHA, Argentina
The ORCID identification number(s) for the author(s) of this article can be found under https://doi.org/10.1002/aenm.202002831.

DOI: 10.1002/aenm.202002831

in the form of charge-separation and -recombination. Hereby, the electronic coupling between electron donor and acceptor and, foremost, the reorganization energies regulate the absolute rate constants. Notably, the rate constant first increases with enlarging driving force. This range is generally referred to as the Marcus normal region of the bell-shaped relationship. When the driving force becomes, however, of the same magnitude as the reorganization energy, the rate constant reaches a maximum. Upon passing the thermodynamic maximum, the highly exothermic region of the parabola is entered, which is generally referred to as the Marcus inverted region. Here, an additional increase of the free energy change results in an actual slowdown of the rate constants. Nature is replicated in non-natural/artificial systems, by means of combining two or more redox-active building blocks to separate charges and transfer them along well-defined redox gradients. In leading examples, charge-separated states with a lifetime of seconds were realized. A contemporary challenge is to manage the transfer of several, that is, two or more charges rather than a single charge. The impact of the latter is substantial in the area of solar fuels. Equally challenging in this area is charge bifurcation and confurcation.

0D, 1D, and 2D nanocarbons in the form of fullerenes/endohedral metallofullerenes (EMFs),[9] single walled carbon nanotubes (SWCNTs),[10] and carbon nanodots (CNDs)[11]/hexabenzocoronenes (HBCs)[12]/graphene[13] represent some of the most promising material families with enormous potential for high-performance applications based on their unprecedented electronic, optical, mechanical, and chemical properties; solar energy conversion, in general, and photovoltaics, as well as photocatalysis, in particular. Next to their rich electrochemistry, most 0D, 1D, and 2D nanocarbons constitute of the rare case of building blocks with very small reorganization energy in charge transfer reactions; smaller than that found in most organics and inorganics, which are used in charge transfer reactions. As a consequence, the unwanted charge recombination (CR) is pushed deep into the Marcus inverted region—vide supra. In addition, their structural rigidity is outstanding as it supports electron–vibronic (e–v) couplings even at temperatures, where other organics and inorganics deactivate via vibrational cooling. At the same time, 0D, 1D, and 2D nanocarbons are ideal targets for investigating fundamental chemical and physical questions such as shape- and charge-dependent binding and release of molecules, charge-transport in confined spaces, and superior sensing of supramolecular interactions. Because of the almost limitless possibilities of constructing both discrete and extended networks of sp–, sp^2–, and sp^3–hybridized nanocarbons, many additional and so far unknown modifications with remarkable properties are imaginable and several examples have been predicted theoretically. Potential drawbacks of SWCNTs, CNDs, and graphene are, in contrast to fullerenes and EMFs, their structural diversity and the lack of control thereof, on one hand, and their instability, on the other hand. For example, to this date, not a single methodology exists that supports synthesis of SWCNT with a single chirality in reasonable quantities. To add to this challenge, single layer graphene requires stabilization to suppress restacking.

Within the large family of porphyrinoid systems, porphyrins (Ps) and (metallo)porphyrins (MPs) enjoy a privileged position in photon- and charge-management.[14] Most notable are intense absorptions in the blue/UV and the red/near-infrared regions in the form of Soret-band and Q-band transitions, respectively, as well as electrochemical and photochemical stability. In addition, their physico-chemical properties are usually fine-tuned by chemical modification of the central metal and/or the peripheral substituents. First, they function as antennas, since they absorb very efficiently light in the visible region of the solar spectrum and, second, once photoexcited, they act as electron donors. Such properties render them suitable to be incorporated into advanced energy materials together with other electro- or photoactive units. In this way, fast and efficient photon- and charge-management, which are fundamental for the fabrication of photovoltaic devices, can be reached.

Even after years of intense investigations, the mixing of 0D, 1D, and 2D nanocarbons, on one hand, and Ps, on the other hand, in advanced energy materials constitutes an interesting and challenging topic.[15–59] Often used in models for multistep electron transfer, the comprehensive understanding of electron donor-acceptor interactions assists in paving the transformation towards artificial photosynthesis: efficient energy conversion and storage units. Considering today's call for alternative, renewable energy sources, efficient energy conversion, and storage units are of great relevance. It all started with the trailblazing contribution from A. L. Moore, T. A. Moore, D. Gust, and coworkers.[60]

The key feature of the Guldi Group's research accomplishments is their ability to assemble advanced energy materials on the nanoscale in a modular fashion and to reach macroscopic scale objects.[61–65] The work has an impact at the fundamental level from the ingenuity of the molecular frameworks designed to achieve specific functions combined with a rigorous physical characterization of the system's photophysics and electrochemistry without losing sight of the ultimate objective of developing integrated solar energy-to-chemical fuel conversion systems, which in the future can be utilized in real devices. A broad range of spectroscopic and microscopic techniques are routinely employed to address aspects that correspond to the optimization and fine-tuning of dynamics and/or efficiencies of charge-separation, charge-transport, charge-shift, and charge-recombination. What stands out is the use of ultrafast spectroscopies, in which any of the aforementioned processes are followed in real-time, commencing with selective excitation of specific building blocks, by electronic absorption and infrared spectroscopies (**Figure 1**).

In this review, we summarize our works in the area of photon- and charge-management, where we were among the first to investigate covalent electron donor-acceptor conjugates built around Ps, on one hand, and 0D, 1D, and 2D nanocarbons, on the other hand. The major challenges in this area, which we faced and addressed in our studies, include:

To establish small reorganization energies in 0D and 1D nanocarbons in short-range intramolecular charge transfer as a means to slow down CR and to ensure charge shift to secondary electron donors or acceptors.
To realize small attenuation factors in 0D nanocarbons in long-range intramolecular charge transfer as a means to move charges over long distances in single steps.
To foster sizeable electron–vibronic couplings in 0D and 1D nanocarbons as a means to accelerate intramolecular charge transfer at room temperature.

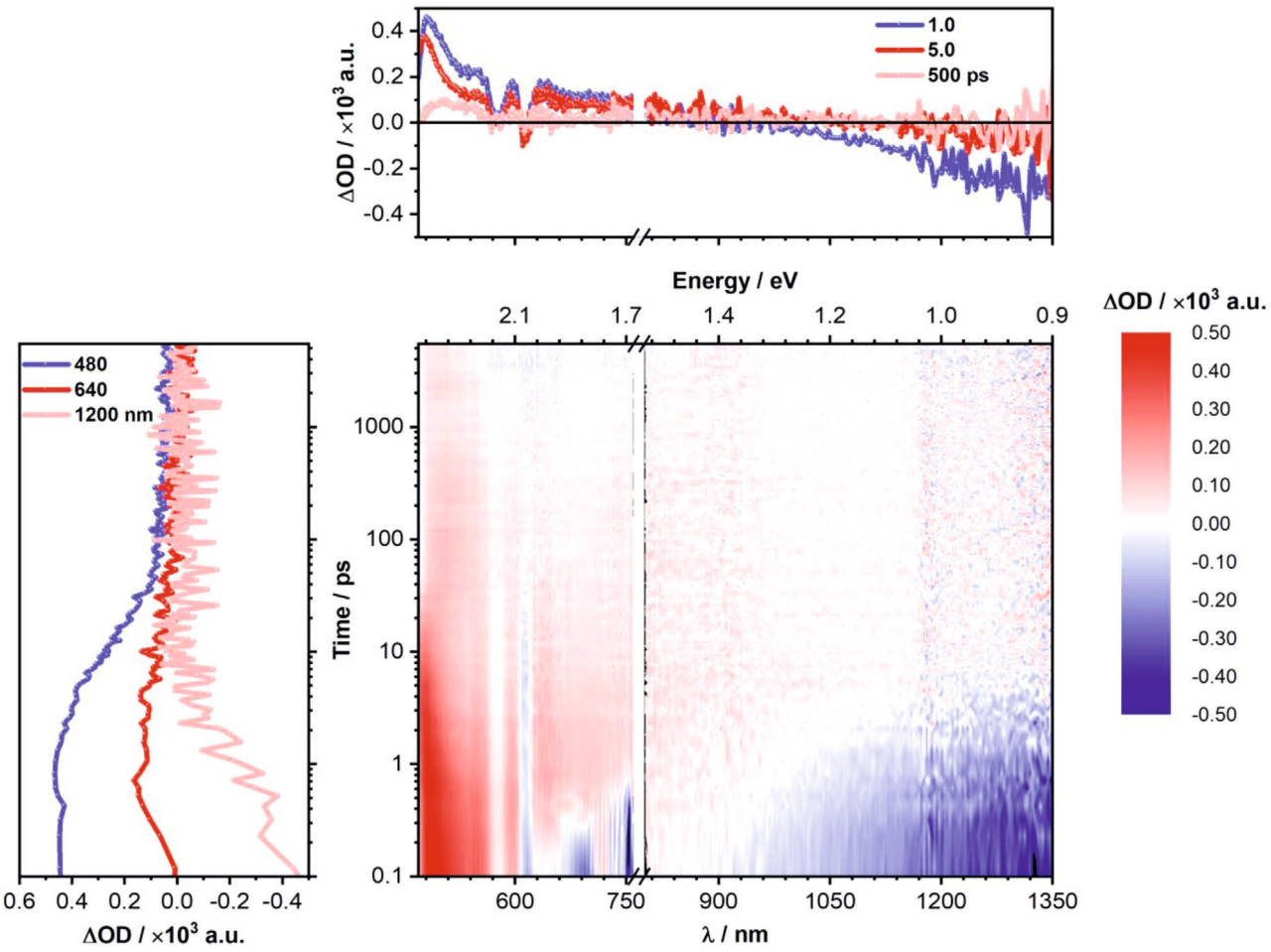

Figure 1. Top right: representative differential absorption spectra (visible and the near infrared region) at time delays of 1.0 ps (blue), 5.0 ps (red), and 500 ps (orange). Bottom left: representative time absorption profiles at 480 nm (blue), 640 nm (red), and 1200 nm (orange), illustrating the dynamics over several time delays in picosecond regime. Bottom right: differential absorption spectra (visible and the near infrared region) of GNP–ZnP–Fc electron donor-acceptor conjugate (**35**) obtained upon femtosecond pump-probe experiments (@ 460 nm) in Ar-saturated THF at room temperature with several time delays of 0 to 5500 ps.

To demonstrate oxidative rather than reductive intramolecular charge transfer in 0D nanocarbons as a means to set-up oxidative photocatalysis.
To explore trapping of charges intramolecularly at the endohedral atoms, ions, or even clusters in 0D nanocarbons as a means to slow down CR.
To gain control over the number of functional groups/defects in 1D and 2D nanocarbons as a means to delocalize charges intramolecularly, rapidly, and efficiently.
To ascertain the use of structurally poor-defined 2D nanocarbon as a means to explore the first steps of photocatalysis.

2. 0D Nanocarbons

2.1. Empty Fullerenes

The 0D structure of empty fullerenes, which are made of alternating hexagons and pentagons of $sp^{2.278}$-hybridized carbon atoms, and, which feature a diameter of 7.8 Å for C_{60}, has stimulated interest in relating their properties to conventional 2D π-systems.[66] Arc-discharge with graphite electrodes is the method of choice for synthesizing gram-quantities of empty fullerenes, which are pure and single isomers in the case of the most abundant C_{60} and C_{70}. Their extraordinary electron accepting properties, which were predicted theoretically and confirmed experimentally, have resulted in noteworthy advances in the areas of light-induced electron transfer chemistry and solar energy conversion.[15,44,45] It is mainly the small reorganization energy and the ability to delocalize electrons that have rendered fullerenes unique for inter- and intramolecular electron transfer processes.[67,68] In essence, multifaceted work has demonstrated that empty fullerenes function predominantly as electron acceptors when integrated together with MPs into energy conversion and storage units.

2.2. EMFs

The versatility of empty fullerenes as a building block for the construction of electron donor-acceptor conjugates has

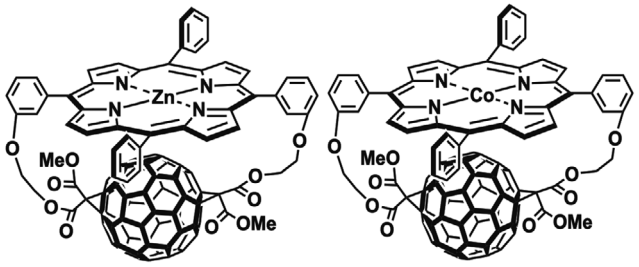

Figure 2. Representative porphyrin conjugates featuring 0D C_{60}: C_{60}—ZnP (**1**) with an electron accepting empty fullerene (C_{60}) and a light harvesting/electron donating zinc (II) porphyrin (ZnP) on the left, and C_{60}-CoP (**4**) with an electron accepting empty fullerene (C_{60}) and a light harvesting/electron donating cobalt (II) porphyrin (CoP) on the right. In THF, charge separation and recombination are 5.5×10^{10} s^{-1} (C_{60}—CoP (**4**)) and 2.5×10^{9} s^{-1} (C_{60}—ZnP (**1**))/4.3×10^{9} s^{-1} (C_{60}—CoP (**4**)), respectively.

motivated many groups to look into enclosing additional atoms, ions, or even clusters into their interior. In this context, noteworthy studies have been reported with EMFs of different types, namely mono-metallofullerenes, di-metallofullerenes, trimetallic nitride fullerenes, etc.[69,70] Doping empty fullerenes with electropositive metals has been demonstrated in an arc generator to yield EMFs. To this date, their production/purification is widely explored and established despite their overall low yields and the large number of isomers. Incorporating different metal species has enabled, for the first time, insights into intramolecular electron transfer processes. Most EMFs retain their spherical structures, but enhanced π-systems and novel chemical/physical properties evolved, which have never been seen for empty fullerenes. Most important is the strong influence of the endohedral atoms, ions, or even clusters on the nature of EMFs endowing them with either electron accepting or electron donating characteristics. As a matter of fact, unlimited access towards EMF-based multi-functional material has been of great interest for emerging applications.

2.3. 0D: Empty Fullerene Porphyrin Conjugates

As far as intramolecular electron transfer reactions are concerned, marked effects were seen in a study, in which we probed a π—π stacked C_{60}—ZnP conjugate (**1**) with van der Waals contacts—**Figure 2**.[71] The short separation of 3.0 Å guaranteed that an intramolecular charge-separation succeeds in virtually any solvent and dominates over the competing energy transfer. The rapid formation and decay of the one-electron oxidized form of ZnP between 670–680 nm and the one-electron reduced form of C_{60} around 900 nm in toluene testified to the charge-separation and -recombination processes, respectively. Now, the systematic change in solvent polarity, for example, from non-polar toluene to polar benzonitrile, provided the powerful means to alter the free energy changes over a wide range. Indeed, a marked acceleration of the charge-recombination rates was seen at smaller thermodynamic driving forces, namely at larger dielectric constants, which corroborated our working hypothesis. To illustrate this, the lifetimes varied over a wide range: 619 ps in toluene to 38 ps in benzonitrile. Most importantly, correlating rate constants with the thermodynamic driving forces and fitting of the resulting parabolic dependence yielded an experimental reorganization energy of 0.86 eV. The delocalization of electrons in C_{60}, provided by its large 3D π-system, resulted in the conclusion that the reorganization energy in the C_{60}—ZnP systems is not receptive towards large changes in the solvent polarity in going, for example, from toluene and THF to benzonitrile. Accordingly, the reorganization energies of the C_{60}—ZnP conjugate are reasonably assumed to be comparable in the different solvents.

In addition, a series of different metalloporphyrins (MP) bearing manganese(III) (**2**), iron(III) (**3**), cobalt (II) (**4**), nickel(II) (**5**), and copper(II) (**6**) were investigated—Figure 2.[72] In all these C_{60}—MP conjugates, a key feature was, once again, the van der Waals distance separating the excited-state electron donating MP from C_{60}. Importantly, this π—π stacking motif emerged as a powerful tool for overcoming the intrinsically fast deactivation of the excited states in MP. The lifetimes of the rapidly and efficiently generated charge-separated state were found to depend on the solvent polarity and on the metal species.

Next, linear arrays were tested, in which a systematic variation of electron donor-acceptor separation between the electron donating ZnP and the electron accepting C_{60} to about 11.9 Å in (**7**), leads to lifetimes of up to 2.7 µs in deoxygenated THF.[73] Notably, several C_{60}—ZnP conjugates, whose electron donor-acceptor distances fall essentially in between these limits, that is, from 3.0 to 11.9 Å, revealed lifetimes that are typically on the order of several tens to hundreds of picoseconds. In THF, the values range from 45 to 398 ps documented some interesting trends: placing the same bridge at different positions of the porphyrin, that is, meso- versus pyrrole-position, and/or using different bridges, that is, ethynylene versus phenyleneethynylene, respectively, impacts the electronic coupling element (V). The electronic coupling decreased monotonically with distance throughout the series: from 415 to 39 cm^{-1}. Likewise, the reorganization energies disclosed differences. They described a fundamental distance dependence, where they first drop from 0.82 eV at 3.0 Å to 0.5 eV at 6.18 Å and after that, they steadily increase to 0.66 eV at 11.9 Å.[74]

But, it is well documented that not only the electronic coupling, but also the attenuation factor is a function of electronic structure and overall architecture of the molecular bridge. Thus, much effort was devoted to designing bridges that facilitate long-range electron transfer reactions. In this context, π-conjugated oligomers were interesting candidates, which led to the investigations of C_{60} and ZnP connected by alkynes (**8**), *p*-phenyleneethylenes (o*p*PE) (**9**), fluorenes (oFl) (**10**), *p*-phenylenevinylenes (o*p*PV) (**11**), etc—**Figure 3**.[74] As a leading example, molecular o*p*PV-bridges, which span electron donor-acceptor distances of up to 38.7 Å, exhibited attenuation factors as low as 0.01 $Å^{-1}$. The reorganization energy was, however, distance invariant between 24.9 and 38.7 Å with 0.72 eV. A major setback of the aforementioned π-conjugated oligomers was the rotation around the single bonds, which connect the individual phenyl units. In short, it caused a deviation from planarity along the oligomer chain. To this end, the most intriguing contribution came from carbon-bridged oligo-*p*-phenylenevinylene (Co*p*PV) bridges (**12**)—Figure 3.[75] Their rigid and flat structure ruled out any deviation from planarity along the oligomer chain. Relative

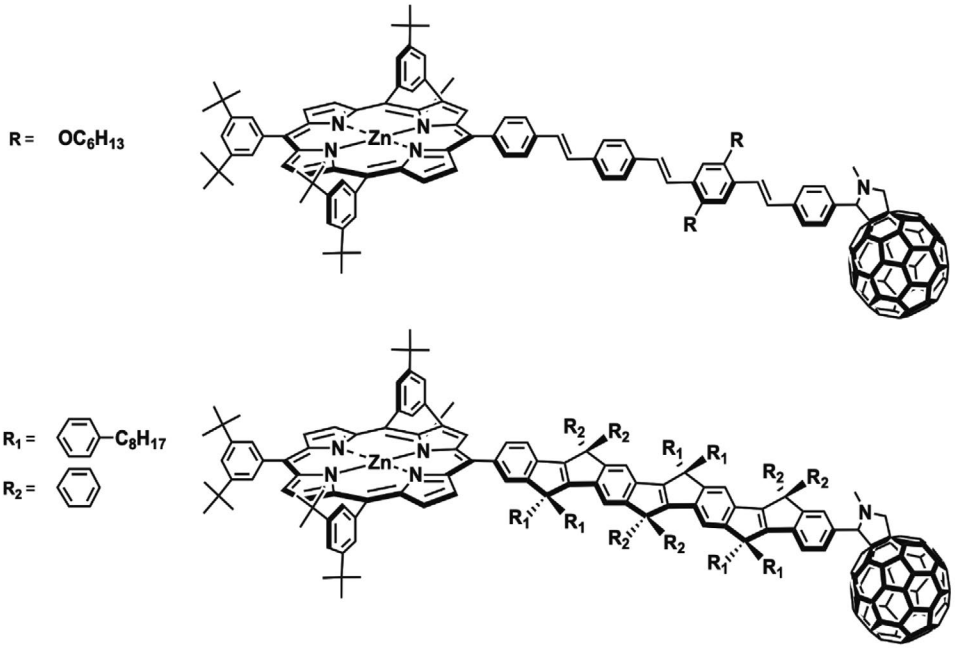

Figure 3. Representative porphyrin conjugates featuring 0D C_{60}: (C_{60}—ZnP)s with an electron accepting empty fullerene (C_{60}) and a light harvesting/electron donating zinc (II) porphyrin (ZnP) linked by a molecular (o*p*PV)$_3$-bridge (**11**) on the top, and a molecular (Co*p*PV)$_3$-bridge (**12**) on the bottom. In THF, charge-separation and recombination are 4.5×10^9 s^{-1} (C_{60}—(o*p*PV)$_3$—ZnP (**11**))/7.1×10^{10} s^{-1} (C_{60}—(Co*p*PV)$_3$—ZnP (**12**)) and 1.2×10^6 s^{-1} (C_{60}—(o*p*PV)$_3$—ZnP (**11**))/5.9×10^9 s^{-1} (C_{60}—(Co*p*PV)$_3$—ZnP (**12**)), respectively.

to a comparable molecular o*p*PV-bridge, both, the electronic coupling element and the reorganization energy were enhanced due to the flatness of the molecular Co*p*PV-bridge with values of 39 cm^{-1} and 0.89 eV, respectively.

Similar effects were also seen for several C_{60}—H_2P conjugates—**Figure 4**.[76–78] An important consideration implies, however, that the 200 mV higher oxidation potential of the $H_2P^{\bullet+}/H_2P$ couple relative to that of $ZnP^{\bullet+}$/ZnP, would allow storing a larger fraction of the excited state energy as chemical potential in the charge-separated state. Slower charge-separation and charge-recombination were logical consequences that stemmed from the energy gap variation in the C_{60}—H_2P versus the C_{60}—ZnP conjugates. For the pyrrole linked C_{60}—H_2P (**13**) and C_{60}—ZnP (**14**) charge-recombination lifetimes of 290 and 50 ps, respectively, were reported.

In a nutshell, our work and that of others[79–84] has been essential to substantiate that, in the combination with MPs, 0D empty fullerenes accept electrons in short- and long-range fashions rather than donate electrons—**Scheme 1**. Key to realize charge separated state lifetimes as long as 2.7 µs has been the full control over the reorganization energies, attenuation factors, and electronic couplings. The former two have been as low as 0.6 eV and 0.01 Å^{-1}, respectively, while the latter reached values of up to 415 cm^{-1}. Similar conclusions have been drawn when (metallo)phthalocyanines, in which the visible light absorption is substantially pushed into the red region of the solar spectrum, are used rather than MPs. The only notable exception among porphyrinoid systems has been a subphthalocyanine (SubPc) linked to C_{60}, in which case SubPcs outcompeted C_{60}s in their effort for accepting electrons

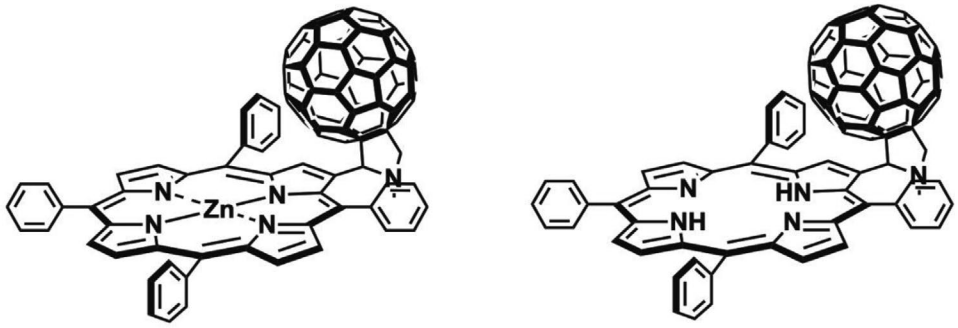

Figure 4. Representative porphyrin conjugates featuring 0D C_{60}: C_{60}—ZnP (**14**) with an electron accepting empty fullerene (C_{60}) and a light harvesting/electron donating zinc (II) porphyrin (ZnP) on the left, and C_{60}-H_2P (**13**) with an electron accepting empty fullerene (C_{60}) and a light harvesting/electron donating free-base porphyrin (H_2P) on the right. In THF, CR is 3.4×10^9 s^{-1} (C_{60}—H_2P (**13**))/2.0×10^{10} s^{-1} (C_{60}—ZnP (**14**)).

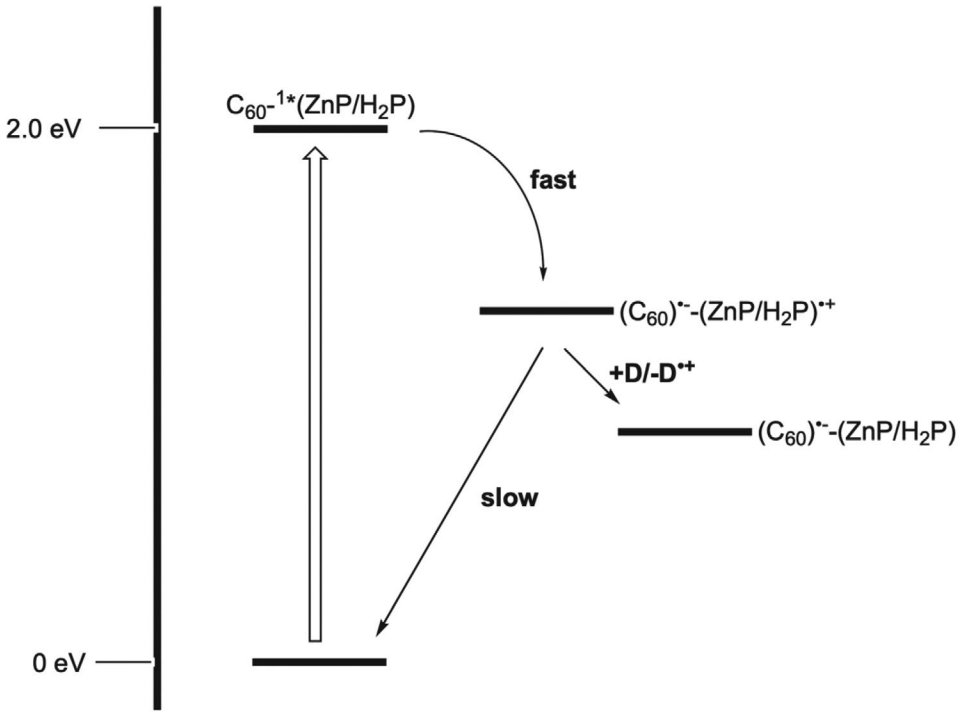

Scheme 1. Energy diagram for empty fullerene porphyrin conjugates highlighting the fast charge-separation and the slow CR stemming from the small reorganization energies of fullerenes in charge transfer reactions and the small attenuation factor to push the latter deep into the Marcus inverted region as well as to enable charge shift to a secondary electron donor (D).

upon photoexcitation.[85] Among the major drawbacks of empty fullerenes is their tendency to dimerize once they are singly-reduced, which creates thermodynamic traps, and, which prevents charge transport. Likewise, their doubly-reduced form should be mentioned; empty fullerenes undergo de-functionalization, which renders them impractical as charge accumulators. A likely solution is to use them as charge mediators rather than charge accumulators.

2.4. 0D: EMF Porphyrin Conjugates

In a pioneering investigation with the $Ce_2@I_h$-C_{80}—ZnP conjugate (**15**), a molecular switching behavior was documented—**Figure 5**. In particular, $Ce_2@I_h$-C_{80}-ZnP (**15**) underwent either reductive electron transfer in non-polar media or oxidative electron transfer in polar media with lifetimes of ca. 0.8 ps and 0.4–0.7 ps, respectively. The transients observed

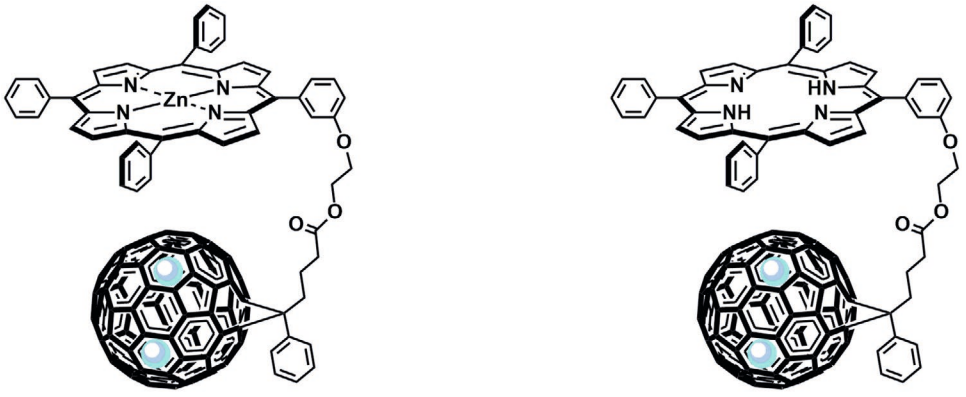

Figure 5. Representative porphyrin conjugates featuring 0D EMFs: $Ce_2@I_h$-C_{80}—ZnP (**15**) (Ce^{3+}s are shown in cyan) with an electron accepting EMF ($Ce_2@I_h$-C_{80}) and a light harvesting/electron donating zinc (II) porphyrin (ZnP) in non-polar solvents or an electron donating EMF ($Ce_2@I_h$-C_{80}) and a light harvesting/electron accepting zinc (II) porphyrin (ZnP) in non-polar solvents on the left, and $Ce_2@I_h$-C_{80}—H_2P (**16**) (Ce^{3+}s are shown in cyan) with an electron accepting EMF ($Ce_2@I_h$-C_{80}) and a light harvesting/electron donating free-base porphyrin (H_2P) on the right. In THF, charge-separation and recombination are 1.3×10^{12} s^{-1} ($Ce_2@I_h$-C_{80}—ZnP (**15**))/5.4×10^{10} s^{-1} ($Ce_2@I_h$-C_{80}—H_2P (**16**)) and 2.4×10^{8} s^{-1} ($Ce_2@I_h$-C_{80}—ZnP (**15**))/> 5.4×10^{10} s^{-1} ($Ce_2@I_h$-C_{80}—H_2P (**16**)), respectively.

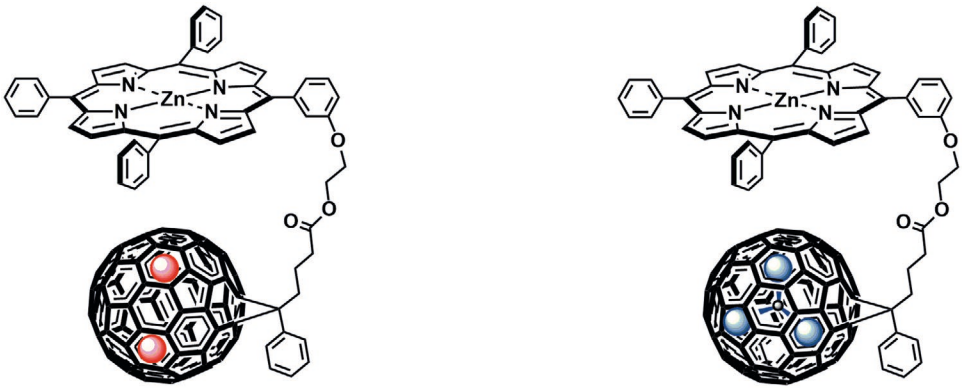

Figure 6. Representative porphyrin conjugates featuring 0D EMFs: $La_2@I_h$-C_{80}—ZnP (**17**) (La^{3+}s are shown in red) with an electron accepting EMF ($La_2@I_h$-C_{80}) and a light harvesting/electron donating zinc (II) porphyrin (ZnP) in non-polar solvents or an electron donating EMF ($La_2@I_h$-C_{80}) and a light harvesting/electron accepting zinc (II) porphyrin (ZnP) in non-polar solvents on the left, and $Sc_3N@I_h$-C_{80}—ZnP (**18**) (Sc_3N^{6+} is shown in blue) with an electron accepting EMF ($Sc_3N@I_h$-C_{80}) and a light harvesting/electron donating zinc (II) porphyrin (ZnP) on the right. In THF, charge-separation and recombination are 1.0×10^{12} s^{-1} ($La_2@I_h$-C_{80}—ZnP (**17**))/1.0×10^{11} s^{-1} ($Sc_3N@I_h$-C_{80}—ZnP (**18**); toluene) and 5.8×10^{9} s^{-1} ($La_2@I_h$-C_{80}—ZnP (**17**))/2.3×10^{10} s^{-1} ($Sc_3N@I_h$-C_{80}—ZnP (**18**); toluene), respectively.

in the near-infrared between 900 and 1200 nm confirmed the one-electron reduced form of $Ce_2@I_h$-C_{80}, while the transient around 850 nm confirmed the one-electron oxidized form of $Ce_2@I_h$-C_{80}. Despite the flexible 2-oxyethyl butyrate spacer, the short distance and higher strength in the electronic coupling between C_{80}/ZnP versus $[Ce_2]^{6+}$/ZnP, the nonadiabatic formation of the $(Ce_2@I_h\text{-}C_{80})^{\bullet-}$—$ZnP^{\bullet+}$, was favored. A closer look reveals the reduction of $[Ce_2]^{6+}$ and not that of C_{80}. This electron transfer mechanism dominated in non-polar media such as toluene and THF with lifetimes of up to 4100 ps. In stark contrast was the behavior in polar-media. In benzonitrile or DMF, the otherwise endergonic level $(Ce_2@I_h\text{-}C_{80})^{\bullet+}$—$ZnP^{\bullet-}$, which is 2.3 eV in non-polar media with respect to the singlet excited state of ZnP (2.1 eV), was stabilized by 0.3 eV. This, in turn, drove its formation with subsequent charge-recombination to afford $^{3*}(Ce_2@I_h\text{-}C_{80})$—ZnP. For the charge-recombination of $(Ce_2@I_h\text{-}C_{80})^{\bullet+}$—$ZnP^{\bullet-}$ in benzonitrile and DMF, the lifetimes were 55 ps and 116 ps, respectively.[86]

Intriguingly, the electron transfer mechanism for the analogous conjugates with H_2P, that is, $Ce_2@I_h$-C_{80}—H_2P (**16**), exhibited, in contrast to the investigation with $Ce_2@I_h$-C_{80}—ZnP (**15**), a rather solvent independent character—Figure 5. The reason for which was the H_2P singlet excited state (1.90 eV), which is 0.2 eV lower in energy than the ZnP singlet excited state (2.10 eV). Notably, it provided less thermodynamic driving forces for the oxidative pathway. The $(Ce_2@I_h\text{-}C_{80})^{\bullet-}$—$H_2P^{\bullet+}$ lifetime was shorter than its formation, hence, could not be fit.[87]

Another important study involved the comparative investigation of two electron donor-acceptor conjugates using isoelectronic EMFs based on an I_h-C_{80} cage, with different types of endohedral guests: $(La_2)^{6+}$ versus $(Sc_3N)^{6+}$—**Figure 6**. In $La_2@I_h$-C_{80}—ZnP (**17**) and $Sc_3N@I_h$-C_{80}—ZnP (**18**), the excited state electron donating ZnPs were linked via 2-oxyethyl butyrate spacers. Even though the combined studies of crystallography and NMR determined a common (6,6)-open addition pattern, the structural characterization gave rise to subtly different conformations, that is, rigid and comparatively flexible structure for $La_2@I_h$-C_{80}—ZnP and $Sc_3N@I_h$-C_{80}—ZnP, respectively. Additionally, the electrochemical measurements implied stronger interactions between I_h-C_{80} and ZnP in $La_2@I_h$-C_{80}—ZnP (**17**). This observation was also supported by DFT calculations, which suggested that in the lowest energy confirmation for $La_2@I_h$-C_{80}—ZnP, the $La_2@I_h$-C_{80} and ZnP assume van der Waals distances. Owing to these subtle changes, the duality of charge-separation properties, that is, reductive and oxidative electron transfer, with solvent polarity was observed in the excited-state for $La_2@I_h$-C_{80} similar to the finding described for $Ce_2@I_h$-C_{80}—vide supra.[88] In contrast to $Ce_2@I_h$-C_{80}—ZnP (**15**), reductive charge transfer was limited to the reduction of I_h-C_{80} without revealing any evidence for any occurring $[La_2]^{6+}$ reduction. Lifetimes of 230 ps in toluene and 170 ps in THF are notably shorter than the 4100 ps found upon $[Ce_2]^{6+}$ reduction in $Ce_2@I_h$-C_{80}—ZnP. In the case of $Sc_3N@I_h$-C_{80}—ZnP (**18**) the oxidative pathway was shut down; regardless of the solvent polarity, $(Sc_3N@I_h\text{-}C_{80})^{\bullet-}$—$ZnP^{\bullet+}$ evolved as the sole product of charge separation (CS).

In an extension, the electron transfer events were investigated between ZnP as electron donor and $Sc_3N@I_h$—C_{80} as electron acceptor over larger distances with center-to-center distances of up to 45 Å—**Figure 7**. The quenched fluorescence quantum yields of $Sc_3N@I_h$-C_{80}—ZnP and the nature of the excited-state deactivation from transient absorption spectroscopy delivered the conclusive evidence of charge-separation over transduction of energy transfer from ZnP (2.1 eV) to $Sc_3N@I_h$-C_{80} (1.5 eV). Kinetic analysis established the evolution of $(Sc_3N@I_h\text{-}C_{80})^{\bullet-}$—$ZnP^{\bullet+}$ with a driving force of 0.63 eV. In terms of charge-recombination for $(Sc_3N@I_h\text{-}C_{80})^{\bullet-}$—$ZnP^{\bullet+}$ in THF and benzonitrile at electron donor-acceptor distances of 33 and 45 Å in $Sc_3N@I_h$-C_{80}—ZnP (**19**) and $Sc_3N@I_h$-C_{80}—ZnP (**20**), respectively, the lifetimes were fit to be in the 1–3 µs regime.[89]

In conclusion, different from the reductive electron transfer, reactivity of 0D empty fullerenes—vide supra—has been our full-fledged investigations on 0D EMFs: Depending on the nature of the MPs, on one hand, and the solvent polarity, on the other hand, electrons have been transferred both ways to either reduce or oxidize EMFs—**Scheme 2**. This clearly stands out in the area of charge transfer with 0D fullerenes. Unique is the ability of EMFs to trap charges in their interior by, for example,

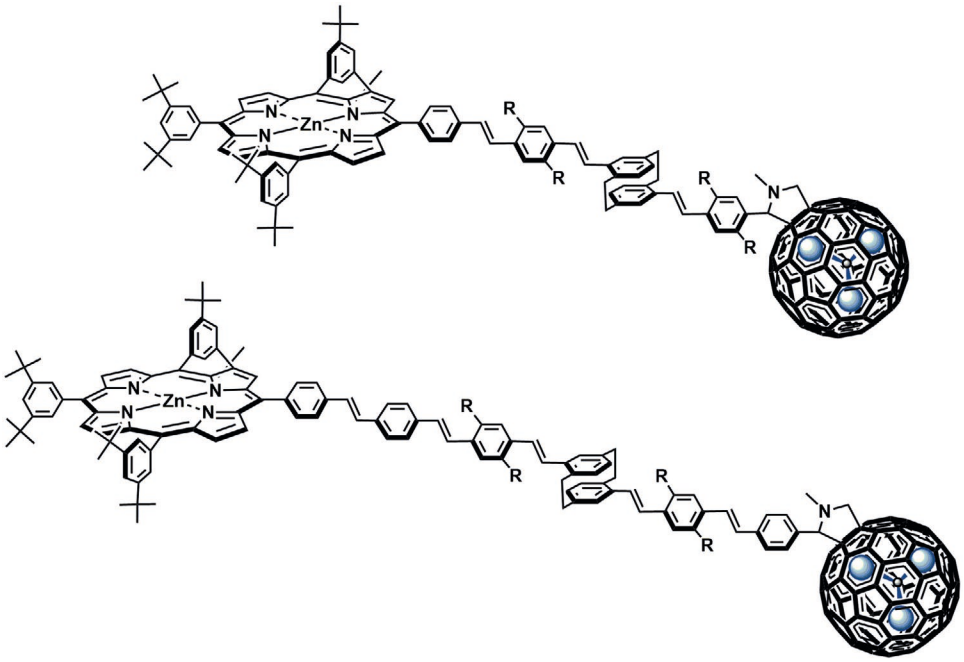

Figure 7. Representative porphyrin conjugates featuring 0D EMFs: $Sc_3N@I_h$-C_{80}—ZnP (**19**) (Sc_3N^{6+} is shown in blue) with an electron accepting EMF ($Sc_3N@I_h$-C_{80}) and a light harvesting/electron donating zinc (II) porphyrin (ZnP) on the top, and $Sc_3N@I_h$-C_{80}—ZnP (**20**) (Sc_3N^{6+} is shown in blue) with an electron accepting EMF ($Sc_3N@I_h$-C_{80}) and a light harvesting/electron donating zinc (II) porphyrin (ZnP) on the bottom (R = $-C_8H_{17}$). In THF, CR is 1.0×10^6 s^{-1} ($Sc_3N@I_h$-C_{80}—ZnP (**19**))/6.6×10^5 s^{-1} ($Sc_3N@I_h$-C_{80}—ZnP (**20**)).

reducing $[Ce_2]^{6+}$; since it enables stabilizing the charge separated states by a factor of about 40 and 100 relative to the reduction of I_h-C_{80} in $La_2@I_h$-C_{80}—ZnP (**17**) and $Sc_3N@I_h$-C_{80}—ZnP (**18**), respectively. A real drawback of EMFs is their low triplet excited state energies, which governs the CR to afford the triplet excited state rather than the ground state. In other words, the underlying driving forces are placed close to the Marcus top region and, in turn, the rate constants are maximal. One possible way to bypass the aforementioned is trapping the charges reductively at the endohedral atoms, ions, or even clusters. But, this comes at the expense of weak electronic coupling, which opens deactivation channels that compete with the CS.

3. 1D Nanocarbons

3.1. SWCNTs

Expanding the delocalized structure of $sp^{2.278}$-hybridized carbon atoms in 0D empty fullerenes and EMFs along 1D by

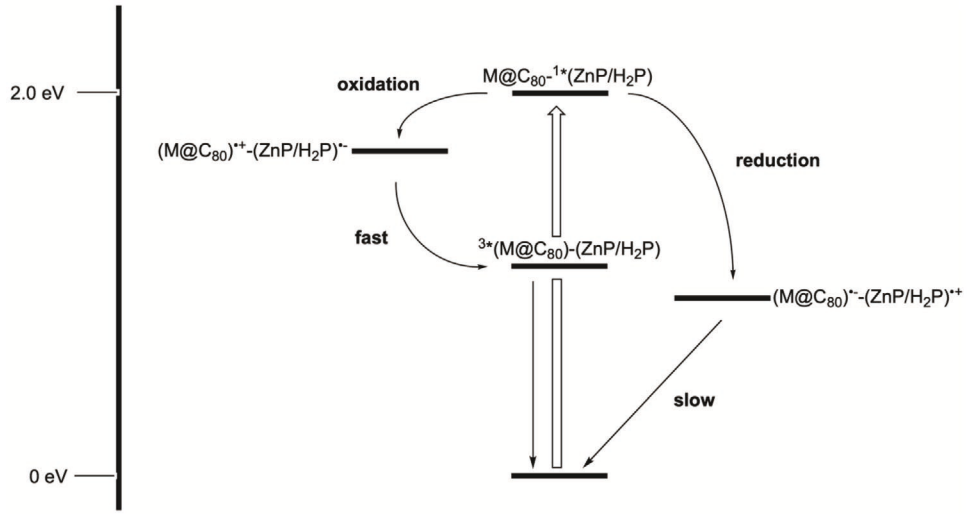

Scheme 2. Energy diagram for EMF porphyrin conjugates highlighting the oxidation of EMFs on the left, and the reduction of EMFs, that is, the reduction of the endohedral atoms, ions, or even clusters, on the right stemming from the fast CS and leading to fast and slow CR, respectively.

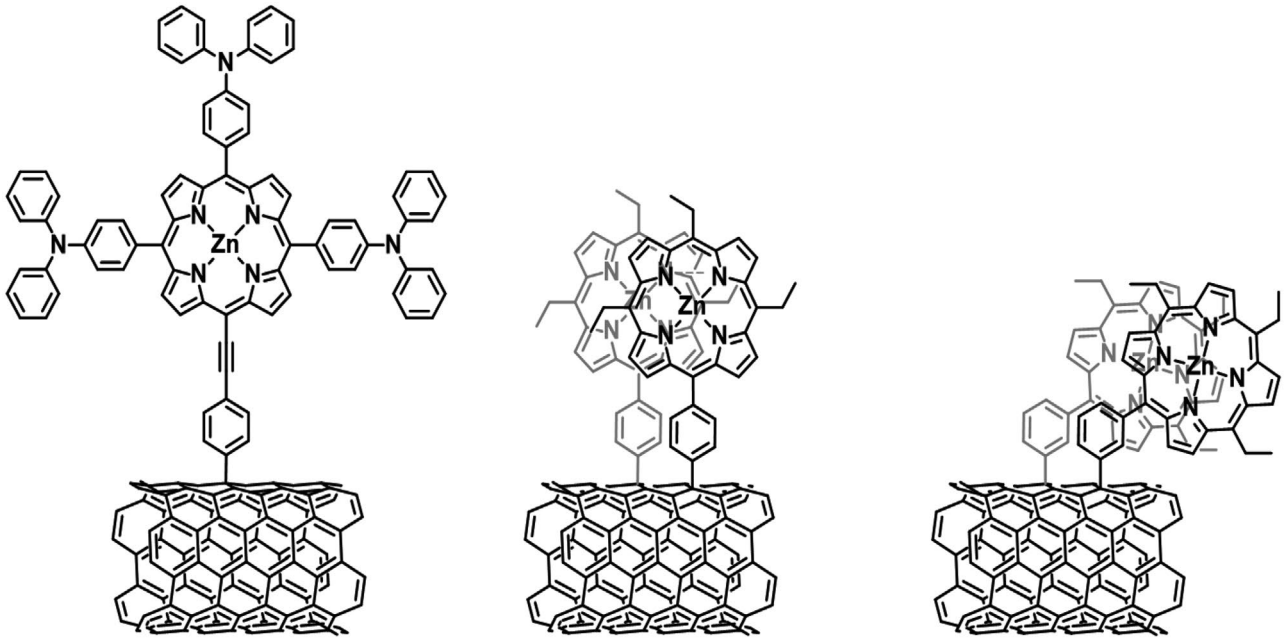

Figure 8. Representative porphyrin conjugates featuring 1D SWCNTs: SWCNT−ZnP (**21**) with an electron accepting SWCNT and a light harvesting/electron donating zinc (II) porphyrin (ZnP) on the left, SWCNT−ZnP (**22**) with an electron accepting SWCNT and a light harvesting/electron donating zinc (II) porphyrin (ZnP) in the center, and SWCNT−ZnP (**23**) with an electron accepting SWCNT and a light harvesting/electron donating zinc (II) porphyrin (ZnP) on the right. In THF, CR is 2.0×10^{11} s^{-1} (SWCNT−ZnP (**21**)). In DMF, CR is 4.2×10^{10} s^{-1} (SWCNT−ZnP (**22**))/2.0×10^{10} s^{-1} (SWCNT−ZnP (**23**)).

means of inserting additional carbon hexagons have produced 1D SWCNTs. Conceptually, 1D SWCNTs reinforce charge-delocalization and charge-transport in a way that 0D empty fullerenes and EMFs could never do. SWCNTs exhibit unique electronic, mechanical, and optical properties. Most prominently, SWCNTs are either small band-gap semiconductors or metals with conductance that reach ballistic dimensions. But, SWCNT syntheses lead to heterogeneous products in terms of chirality, diameter, and length. Myriads of structural defects go hand-in-hand with the presence of catalyst particles and the fact that SWCNTs bundle. In short, synthesis, sorting, and individualization of SWCNTs are major challenges toward future applications. Several techniques have highlighted the fact that semiconducting SWCNTs are intrinsically p-type doped and, in turn, donate electrons rather than accept electrons. Only discernible are these properties for SWCNTs that are debundled, individualized, and stabilized, often in solution. Typically, they are poorly soluble in many media. Large SWCNT bundles originate from attractive interactions such as π–π stacking and London dispersion forces. Over the last 15 years, a myriad of studies regarding the covalent functionalization of SWCNTs with different Ps have been reported.[90–94]

3.2. 1D: SWCNT Porphyrin Conjugates

In one of the functionalization approaches, a ZnP, which was functionalized at three meso-positions with triphenylamine entities as electron donors, was attached to SWCNTs at the remaining ZnP meso-position—**Figure 8**. To this end, the SWCNT−ZnP (**21**) conjugate was synthesized by a Sonogashira coupling under microwave irradiation conditions.[95] The advantages of the covalent approach were counterbalanced by the defects or detrimental disruption of the π-conjugated structure of SWCNTs, which strongly impact the optical and electronic properties. In Raman spectra, the D-mode intensity allowed insights into the level of covalent functionalization. The down-shifts present in the G-, D-, and 2D-modes prompt to n-type doping in the form of charge-transfer interactions between SWCNTs and ZnP. In general, strong electronic communication between SWCNTs and ZnP—even in the ground state—was deduced from broadened and significantly red-shifted absorption features of SWCNT−ZnP relative to pristine SWCNTs. The presence of a quenched ZnP fluorescence in SWCNT−ZnP (**21**) hint at the occurrence of additional excited state deactivation such as electron transfer and/or energy transfer. Furthermore, the polarity of the solvent played a role in the fluorescence quenching mechanism. For SWCNT−ZnP (**21**), in an apolar solvent such as THF, the fluorescence quenching was notably weaker than in the more polar solvent NMP with 68%. This suggested that electron transfer rather than energy transfer was the main deactivation channel in the SWCNT−ZnP (**21**) conjugate. The formation of $SWCNT^{\bullet-}$−$ZnP^{\bullet+}$ after photoexcitation of ZnP was witnessed by recording the fingerprints of one-electron oxidized form of ZnP and one-electron reduced form of SWCNTs. Importantly, due to the occurrence of a competitive charge-separation process, the recovery of the excitonic maxima in the conjugate was much faster relative to what was seen for pristine SWCNTs. The corresponding lifetimes for SWCNT−ZnP (**21**) and just SWCNTs were 5 and 33 ps, respectively.

A similar trend was also discerned for other SWCNT−ZnP conjugates, where ZnP was covalently grafted to the SWCNT sidewalls by direct aryl radical addition reaction with a meta- or

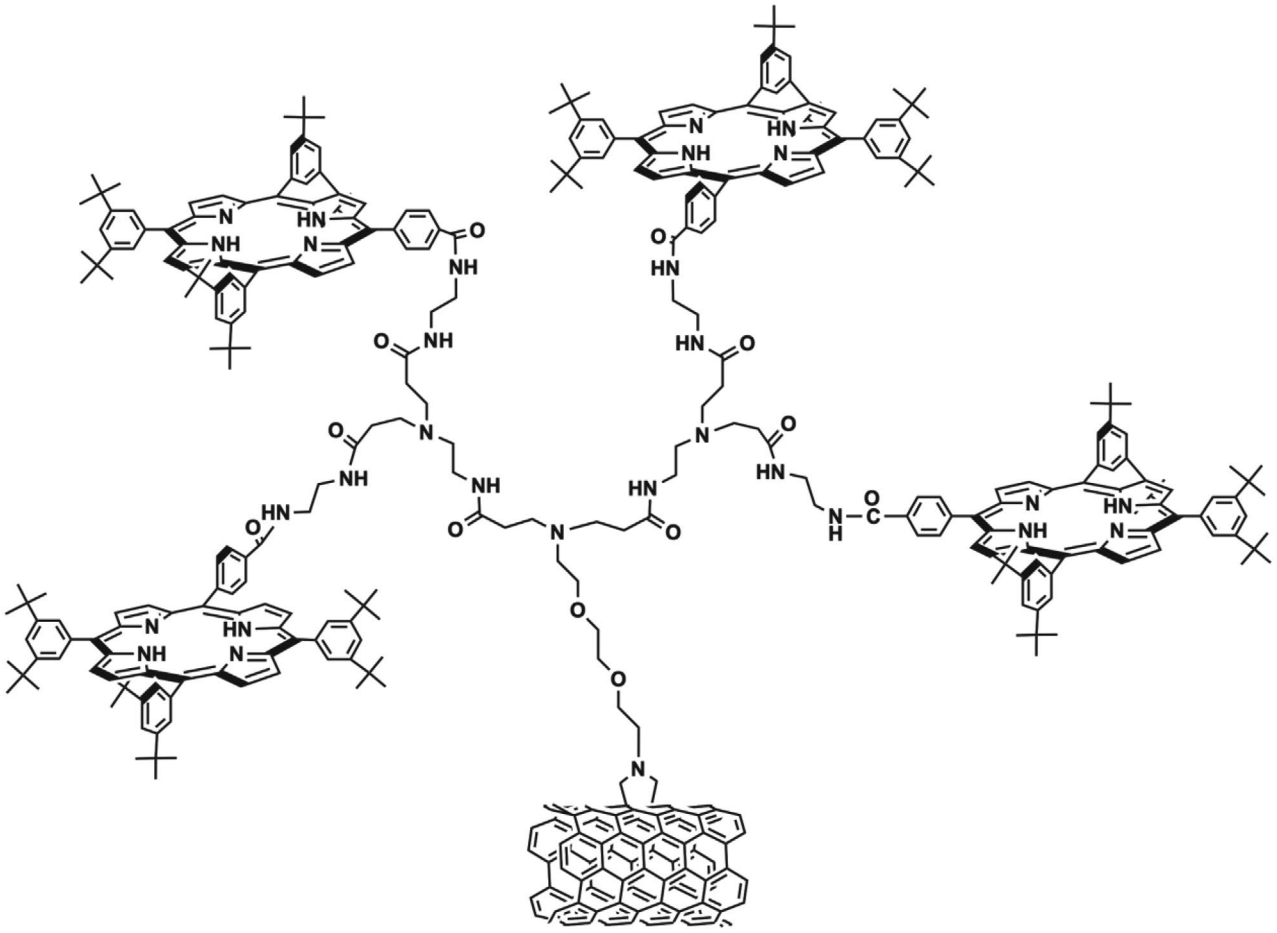

Figure 9. Representative porphyrin conjugates featuring 1D SWCNTs: SWCNT−$(H_2P)_4$ (**24**) with an electron accepting SWCNT and a light harvesting/electron donating free-base porphyrin (H_2P). In THF, CS and recombination are 1.5×10^{10} and 2.9×10^6 s^{-1}, respectively.

para-phenylene linker—Figure 8.[96] Specifically, the lifetimes were remarkably longer due to the weaker electronic coupling through the meta-linkage (SWCNT−ZnP (**23**)) with 49 ps than through the para-linkage (SWCNT−ZnP (**22**)) with 24 ps.

Next, the focus was shifted to enhance the light harvesting of H_2P in SWCNT−$(H_2P)_4$ conjugates (**24**), in which four H_2Ps were linked to the periphery of the dendrimers—**Figure 9**.[97] Consequently, absorptions of both, that is, SWCNTs and H_2Ps, were discernable in the absorption spectra. Furthermore, Raman spectra substantiated the covalent functionalization between SWCNTs and $(H_2P)_4$ by means of the presence of an appreciable stronger D-band in the SWCNT−$(H_2P)_4$ conjugates (**24**) relative to what the observations made for pristine SWCNTs. It should be noted that the D-band was not affected by the dendrimer formation lacking H_2Ps. Turning to fluorescence spectroscopy of SWCNT−$(H_2P)_4$ (**24**), a significant fluorescence quenching of the H_2P-centered features was interpreted in terms of excited state interactions between SWCNTs and $(H_2P)_4$. The respective fluorescence kinetics was composed of two fluorescent components, namely a short-lived (0.04 ± 0.01 ns) and a long-lived (8.6 ± 1.2 ns) component. The latter is in sound agreement with that seen for pristine H_2P (9.5 ± 0.5 ns) and implies lack of interactions between H_2P and SWCNTs. A possible explanation was argued with the remote location of some H_2Ps relative to SWCNT as a result of the dendritic structure of the $(H_2P)_4$ function. Finally, transient absorption spectroscopy enabled an assignment of the excited state species. SWCNT−$(H_2P)_4$ (**24**) was subject to fast charge-separation ((1.5 ± 0.5) x 10^{10} s^{-1}) after H_2P photoexcitation to yield SWCNT$^{\bullet-}$−$(H_2P)_4^{\bullet+}$, whose presence was verified by the respective fingerprint absorption features. Important from a kinetic perspective was the fact that the rapid decay of the H_2P singlet excited state was linked to an intramolecular charge-separation.

In prior work, which was about an SWCNT−H_2P conjugate (**25**) with just one H_2P rather than four H_2Ps per linker, the same trends were established—**Figure 10**.[98] The weaker H_2P absorption, due to fewer H_2Ps, rendered, however, the investigations very challenging. For example, the presence of SWCNTs marginally modified the excited state dynamics and/or lifetimes in the SWCNT−H_2P conjugate (**25**): a fluorescence lifetime of 10.4 ± 0.5 ns for H_2P. In the case of the SWCNT−H_2P conjugate, the corresponding lifetime was 5.2 ± 0.5 ns. Nevertheless, transient absorption measurements, which were conducted with SWCNT−H_2P (**25**), yielded the characteristic absorptions of the one-electron oxidized form of H_2P concomitant with the 50 ps decay of the H_2P singlet excited state.

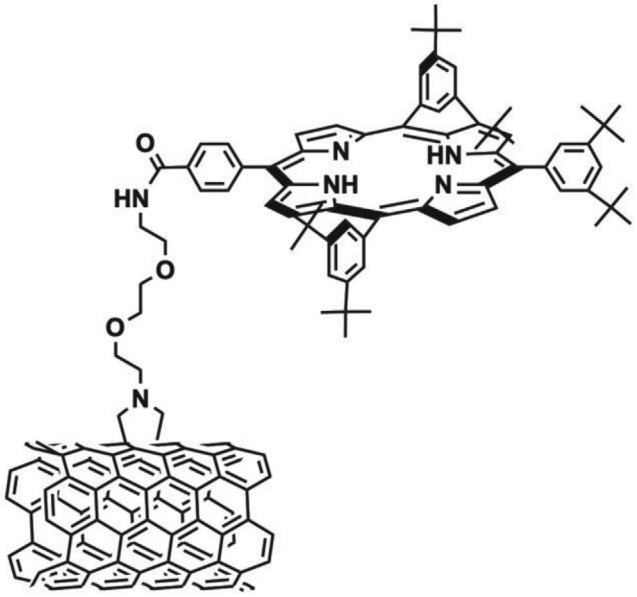

Figure 10. Representative porphyrin conjugates featuring 1D SWCNTs: SWCNT−H_2P (**25**) with an electron accepting SWCNT and a light harvesting/electron donating free-base porphyrin (H_2P). In THF, CR is 2.0×10^{10} s^{-1}.

In a comparative assay, two different SWCNT−ZnP conjugates were tested—**Figure 11**. In SWCNT−ZnP (**26**), a single ZnP was attached per functional group to SWCNTs, whereas in SWCNT−$(ZnP)_2$ (**27**), a first-generation dendron bearing two ZnPs was attached to the SWCNTs.[99] In this particular case, SWCNT functionalization with a ZnP-dendron was carried out by means of click chemistry. Raman spectroscopy with SWCNT-ZnP (**26**) and SWCNT−$(ZnP)_2$ (**27**) allowed detection of a significant increase in the relative intensity of the D-band relative to pristine SWCNTs. Sizeable ground state interactions between SWCNT and ZnP perturbed the absorption spectra of SWCNT-ZnP (**26**) and SWCNT−$(ZnP)_2$ (**27**). In the excited state, conclusions about interactions were drawn from a strong fluorescence quenching and a fast ZnP excited state decay. Both were rationalized as a consequence of charge-transfer interactions. Unambiguous proof for charge-separation came from transient absorption measurements. The lifetime of charge-separated states in SWCNT-ZnP (**26**) (820 ps) and SWCNT−$(ZnP)_2$ (**27**) (200 ps) were, however, marginally changed by the presence of the different spacers that link ZnPs with SWCNTs.

In summary, our work and that of other groups around the globe[100–103] have pioneered the reductive electron transfer reactivity of 1D SWCNTs despite their p-type nature—**Scheme 3**. Surprising to us were CR dynamics on the order of tens of picoseconds, which were, in fact, (much) faster than those found in most conjugates featuring 0D empty fullerene/EMFs. This clearly contradicts a charge delocalization and/or charge transport involving SWCNTs. A setback is, however, the fact that true charge-delocalization and charge-transport along the π-extended network of carbon atoms in SWCNTs has failed to this date. The current belief is that structural defects in the form of sp^3–hybridized carbons are detrimental and need to be avoided. Such structural defects are likely to originate, on one hand, from the SWCNT synthesis and, on the other, the SWCNT functionalization. Albeit challenging the former is manageable, the latter is essential to link the Ps to SWCNTs. Metallic SWCNTs might offer new pathways(!).

4. 2D Nanocarbons

4.1. CNDs

Lots of examples of luminescent, colloidal, and carbon-based materials, which have been synthesized in solution, have been reported under the umbrella term "CNDs". In contrast to the well-defined 0D empty fullerenes and EMFs, on one hand, and 1D SWCNTs, on the other hand, the precise structural characterization of CNDs still constitutes a tremendous challenge. Strictly speaking, CNDs are nanocarbons with (partially)

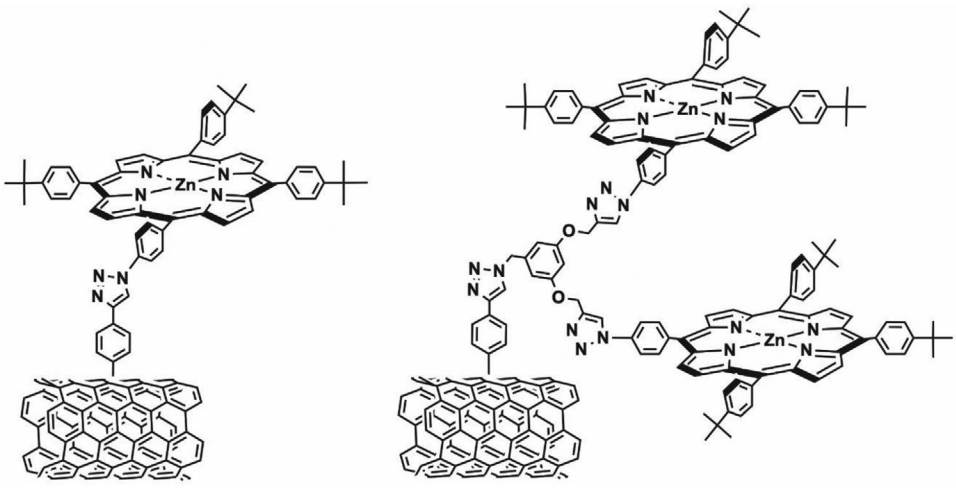

Figure 11. Representative porphyrin conjugates featuring 1D SWCNTs: SWCNT−ZnP (**26**) with an electron accepting SWCNT and a light harvesting/electron donating zinc (II) porphyrin (ZnP) on the left, and SWCNT−$(ZnP)_2$ (**27**) with an electron accepting SWCNT and a light harvesting/electron donating zinc (II) porphyrin (ZnP) on the right. In DMF, CR is 1.2×10^9 s^{-1} (SWCNT−ZnP (**26**))/5.0×10^9 s^{-1} (SWCNT−$(ZnP)_2$ (**27**)).

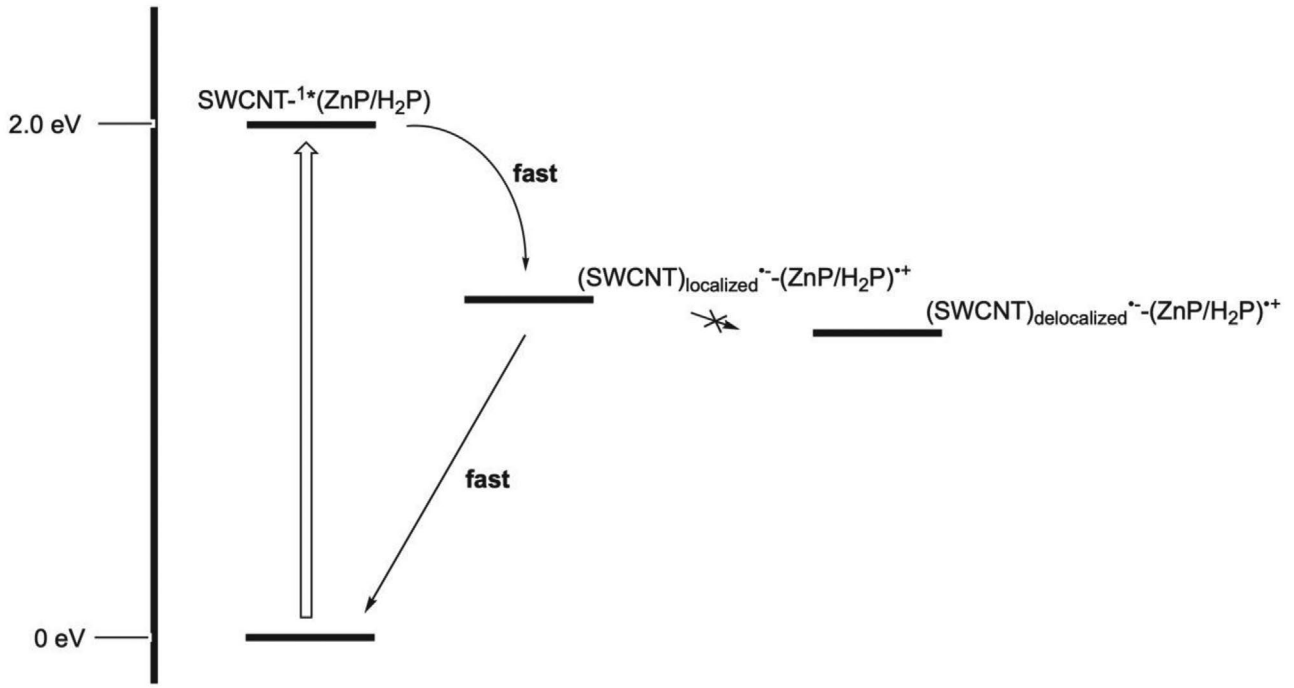

Scheme 3. Energy diagram for SWCNT porphyrin conjugates highlighting the fast CS and the fast CR stemming from the suppression of charge delocalization.

amorphous structures and high heteroatom content. In much of our own work, pressure-synthesized CNDs, for which citric acid and urea are used as inexpensive and biobased precursor materials, lie at the center of attention. Despite the aforementioned, CNDs have attracted a mounting interest: CNDs are a readily available, non-toxic, and tailorable carbon-based nanomaterial. Notable are studies, in which CNDs have been probed with success in terms of reductive and oxidative electron transfer. Among the many remarkable CND properties, their luminescence stands out as very likely to be their most striking optical feature.[104–110]

4.2. Hexa-peri-hexabenzocoronenes

Less amorphous than CNDs are HBCs. HBCs with their extended network of carbons have evolved, on their own merits, as a particularly interesting class of nanocarbon building blocks. For example, their high symmetry, small size, and extended π-system, etc. all renders them interesting not only for chemistry but also for materials science. An interesting aspect will, undoubtedly, be the large HOMO-LUMO gap of HBCs, despite an overall large conjugated π-system. A closer look at the electron distribution has shown that the presence of Clar-sextets is responsible for the interrupted π-conjugation.[25,51,111]

4.3. Graphene Nanoplate (GNP)

Upon pushing the in-plane π-extension of HBCs 2D graphene has been reached. It is constituted of a single atomic layer of sp^2–hybridized carbon in the form of a hexagonal lattice and is best described as a zero-gap material, which conducts electrons like a metal. Given the outstanding properties of this 2D honeycomb lattice in terms of its electrical conductivity and mechanical strength, tremendous research efforts have been invested in the production of defect-free and band-gap tailored graphene sheets; top-down or bottom-up. In fact, the latter has been the basis for a myriad of applications, especially in the area of photovoltaics, either in the form of a transparent conducting electrode or an active component in combination with appropriate organic counterparts such as conjugated polymers. In the current context, we wish to refer to GNPs.[13,112,113,114]

4.4. 2D: CND Porphyrin Conjugates

Strong intramolecular charge-transfer interactions were observed in CND–H$_2$P conjugates (**28**), both in the ground and in the excited state, in H$_2$O/THF 1:1 solutions—**Figure 12**.[115] The

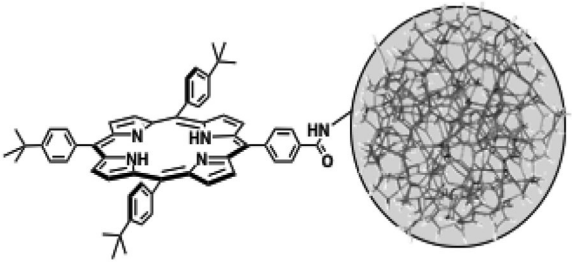

Figure 12. Representative porphyrin conjugate featuring 2D CNDs: CND–H$_2$P (**28**) with an electron accepting CND and a light harvesting/electron donating free-base porphyrin (H$_2$P). In H$_2$O/THF (1:1 v/v), CS and biphasic recombination are >1 × 10^{12} and 1.59 × 10^{11}/4.44 × 10^9 s^{-1}, respectively.

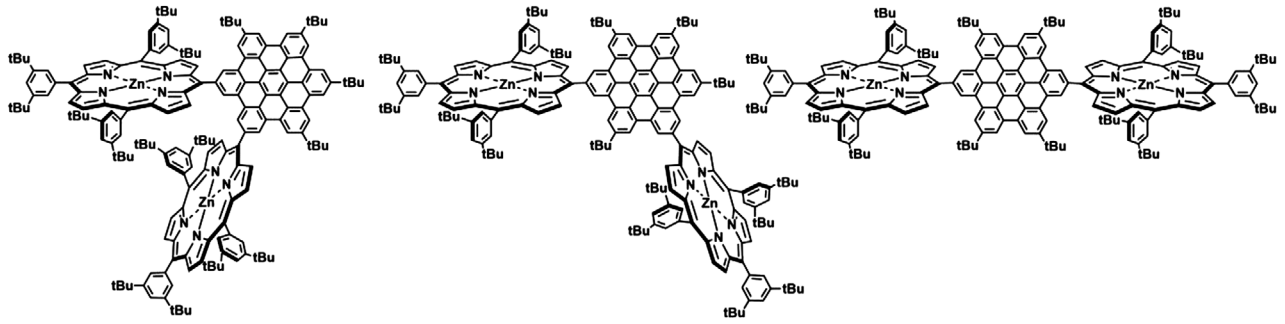

Figure 13. Representative porphyrin conjugates featuring 2D HBCs: ortho-(ZnP−HBC−ZnP) (**29**) with light harvesting ZnPs and a mediating HBC on the left, meta-(ZnP−HBC−ZnP) (**30**) with light harvesting ZnPs and a mediating HBC in the center, and para-(ZnP−HBC−ZnP) (**31**) with a light harvesting ZnPs and a mediating HBC on the right.

Soret-band absorptions of the H_2P were found to be broadened and red-shifted by about 30 nm in comparison to a H_2P-reference, and Q-band absorptions red-shift from 518, 555, 581, and 636 nm to 523, 556, 597, and 650 nm, respectively. Furthermore, CND-centered absorptions were subject to a 6 nm blue-shift in the CND−H_2P conjugate (**28**), when compared with bare CNDs. These results pointed to strong electronic communications between the CNDs and H_2P in the ground state. As a matter of fact, these were favored by their close proximity, which stem from their covalent attachment. Translation of these interactions to the excited state resulted in a 50% quenching of CND emissions and an 80% quenching of H_2P fluorescence in the CND−H_2P conjugate (**28**), in comparison to the individual components. Notable was a 6 nm red-shift of the H_2P fluorescence features. The efficient excited state electronic communication within the conjugate enabled a rich excited state activity. For example, an intramolecular energy transfer process followed the selective CND excitation at 300 nm, which afforded a sizeable H_2P fluorescence. On the other hand, selective H_2P excitation at 422 nm triggered an intramolecular, ultrafast electron transfer from the H_2P to the CNDs. This led to a charge-separated state, which recombined biphasically with lifetimes of 6.3 and 225 ps to reinstate the ground state.

4.5. 2D: Hexabenzocoronene Porphyrin Conjugates

In HBC–ZnP conjugates, in which ZnPs were geometrically arranged in ortho- (**29**), meta- (**30**), and para-position (**31**) around the HBC, ground-state interactions were discernible in form of split Soret-band absorptions—**Figure 13**.[116] The splitting increased along with the substitution pattern, namely it was the weakest in the ortho-(ZnP−HBC−ZnP) conjugate and the strongest in the para-(ZnP−HBC−ZnP) conjugate. The fluorescence was solely ZnP-centered, indicating a highly efficient unidirectional energy transfer from the HBCs to the ZnPs.

The same energy transfer was also proposed to happen in several ethynyl-bridged HBC−(metallo)porphyrin conjugates—**Figure 14**.[117] Introducing ethynyl-bridged HBCs at the meso position of the ZnPs and H_2Ps lowered the symmetry and split/energetically stabilized the electronic states. The latter was also reflected in broadened and red-shifted Soret- and Q-band absorptions. In transient absorption measurements, excited-state deactivation via multiple singlet excited states and consecutively triplet excited states prompted the complexity of the conjugates, which was introduced by the functionalization. In case of a HBC−ZnP−ZnP−HBC array (**33**), the absorptive and

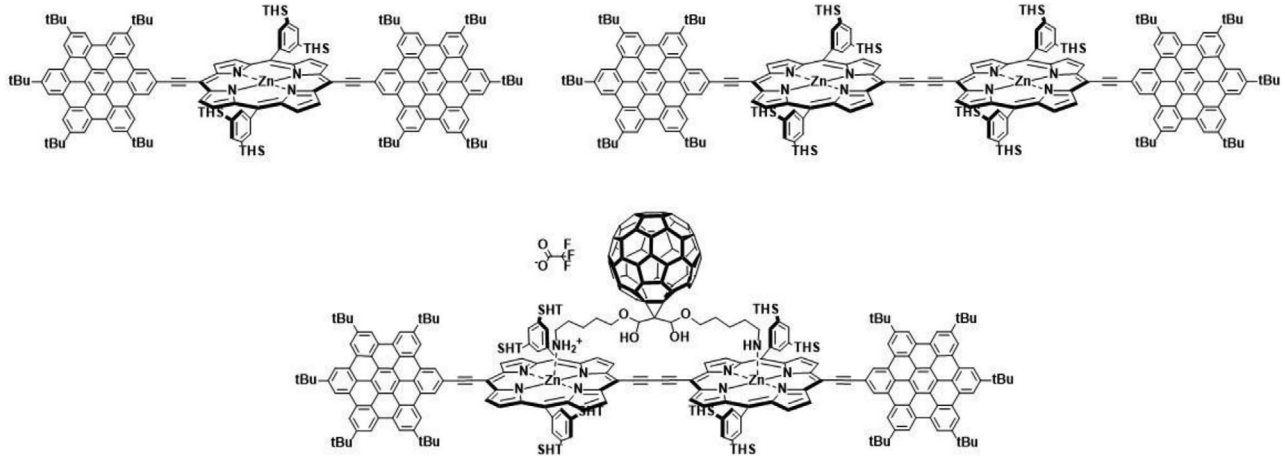

Figure 14. Representative porphyrin conjugates featuring 2D HBCs: HBC−ZnP−HBC (**32**) and HBC−ZnP−ZnP−HBC (**33**) with light harvesting ZnPs and mediating HBC on the top, and (HBC−ZnP−ZnP−HBC)−C_{60} (**34**) with light harvesting/electron donating ZnPs, light harvesting HBC, and an electron accepting C_{60} on the bottom. In benzonitrile, CS and recombination are 0.25–1.25 × 10^{12} and 1.05–2.63 × 10^9 s^{-1} ((HBC−ZnP−ZnP−HBC)−C_{60} (**34**)), respectively.

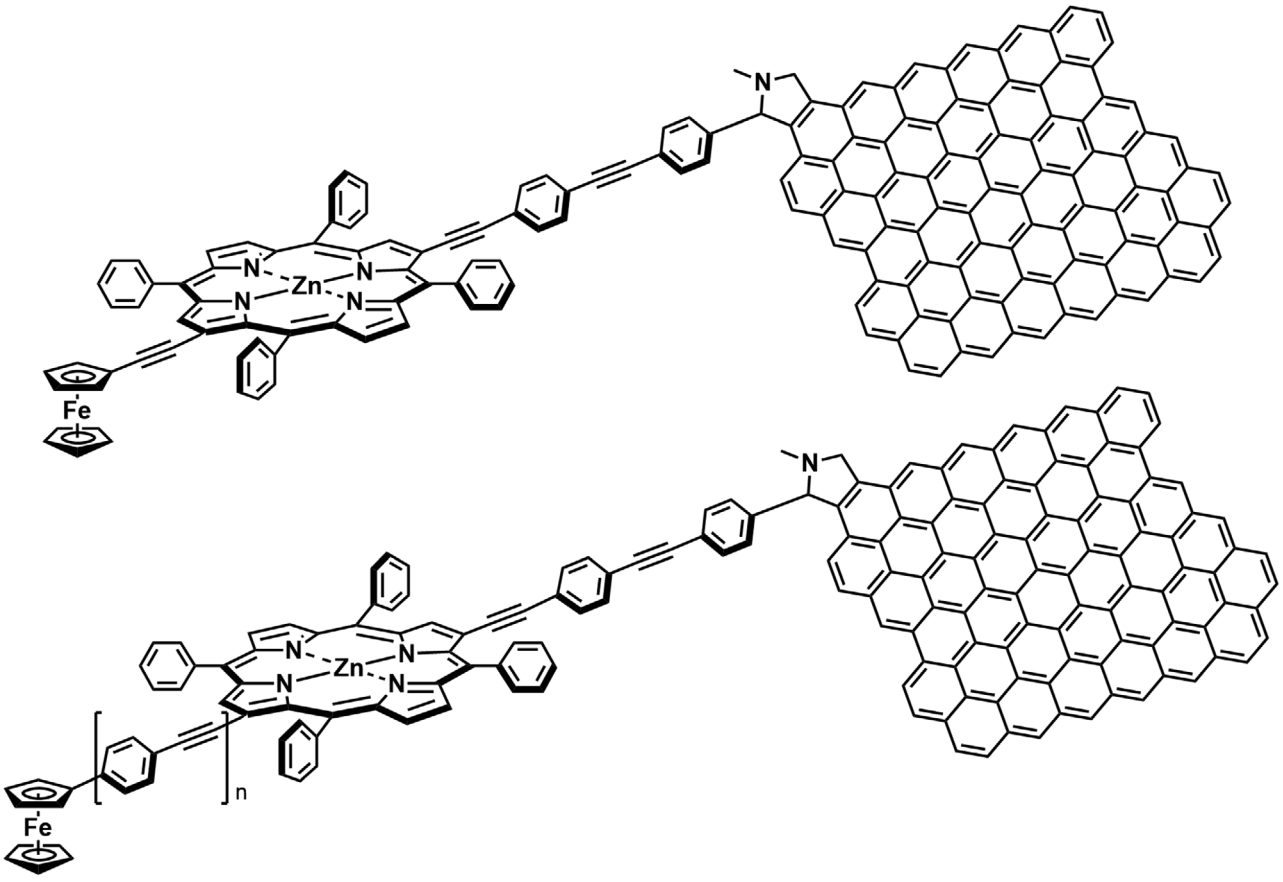

Figure 15. Representative porphyrin conjugates featuring 2D GNPs: GNP—ZnP—Fc (**35** and **36**) with an electron accepting GNP, light harvesting and electron accepting/donating zinc porphyrin (ZnP), and secondary electron donating ferrocene (Fc). In THF, CR is $< 10^8$ s^{-1} (GNP—ZnP—Fc (**35**))/$<10^8$ s^{-1} (GNP—ZnP—Fc (**36**)).

fluorescent features were manually controlled with the help of bidentate ligands. For example, the use of bis(aminoalkyl)-substituted fullerene imposed panchromatic absorptions from 350 nm to beyond 800 nm. Notably, the complexation had an impact on the dihedral angle between the ZnPs, which are individually tuned by the length of the ligand. For bis(aminoalkyl)-substituted fullerene, the dihedral angle is close to 0°. The consequence was a unit efficient energy transfer from the HBCs to the ZnPs followed by a charge-separation from the ZnP to C_{60} in **34**. The charge-recombination lifetimes varied as a function of the center-to-center distance between electron donor and acceptor and ranged from 380 to 950 ps.

4.6. 2D: GNP Porphyrin Conjugates

One of the several, yet challenging approaches is the covalent functionalization of graphene to realize versatile electron donor-acceptor systems.[118,119] Notably, microwave-produced few-layered graphene was used for functionalization and is referred to as GNPs. By employing a strategic combination of the Sonogashira coupling and the Prato–Maggini reaction, a number of GNP—ZnP and GNP—ZnP—Fc electron donor-acceptor conjugates (**35** and **36**) were synthesized—**Figure 15**.[120,121] X-ray photoelectron spectroscopy and Raman mapping combined with imaging were employed to demonstrate successfully the covalent functionalization of GNPs. One of the highlights was the systematic variation of distances between the GNPs, ZnPs, and Fcs by employing oligo-*p*-phenyleneethynylenes of variable lengths to study electron transfer events over long distances. For both, ground and excited state, ZnP was used as a probe. Strong electronic communication was correlated with the changes in absorption features. Here, broadened and red-shifted Soret band absorptions went hand-in-hand with the quenched ZnP fluorescence. From the excited state dynamics upon selective ZnP excitation the instantaneous formation of two short-lived, charge-separated states as intermediates, namely $GNP—ZnP^{\bullet-}—Fc^{\bullet+}$ and $GNP^{\bullet-}—ZnP^{\bullet+}—Fc$ was corroborated. Certainly, the rate of the charge-separation exhibited notable dependences on the length of the oligo-*p*-phenyleneethynylene bridges separating GNP and ZnP, on one hand, as well as ZnP and Fc, on the other hand. Of great importance was the fact that cascades of charge-shift events generated long-lived $GNP^{\bullet-}—ZnP—Fc^{\bullet+}$ charge-separated states with lifetimes in the nanosecond time range featuring a GNP-delocalized electron and the one-electron oxidized form of Fc as one of the final products.[122]

In short, controlling 2D GNPs in electron donor-acceptor conjugates has led to the exploration of 2D CNDs and 2D HBCs. Among them, only 2D GNPs and partially amorphous 2-D

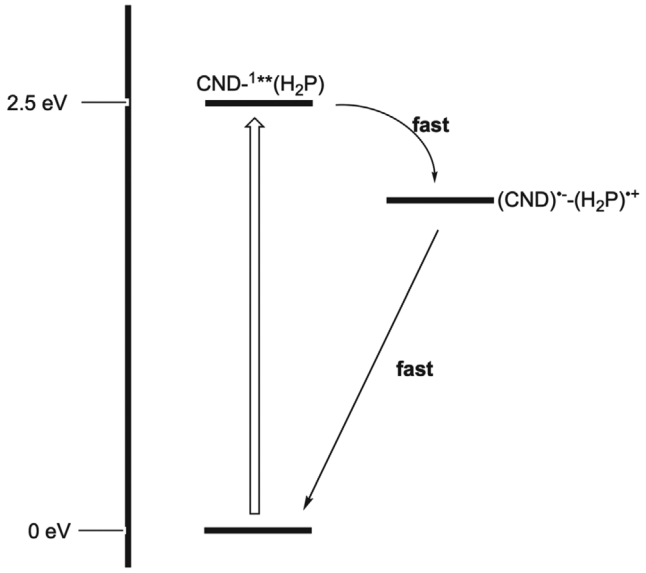

Scheme 4. Energy diagram for CND porphyrin conjugates highlighting the fast CS and fast CR.

CNDs when linked to MPs have participated in electron transfer reactions—**Scheme 4**. Although only a single study with CNDs exists, the corresponding fast CR reflects a general trend made with electron donors other than MPs. Non-amorphous 2D HBCs have been developed into versatile platforms, but to this date, only energy transfer has materialized. CNDs are easy to be produced and bio-compatible, which renders them highly relevant for many emerging applications including photocatalytic proton reduction. The complex, but not completely deciphered, structure of CNDs necessitates, however, a multifaceted strategy to investigate their fundamental electronic structure and to establish structure-property relationships. Nevertheless, the fact that a CND standard is much needed at this point in time constitutes a major drawback. It is only through probing a CND standard that charge transfer bottlenecks become avoidable. Among these bottlenecks is the question if the largely amorphous character of CNDs is advantageous or disadvantageous. An initial study with graphene quantum dots might be a step in the right direction. The setback for GNPs is similar to that discussed for SWCNTs, since true charge-delocalization and charge-transport along the π-extended network of carbon atoms in GNPs has not been realized. Again, structural defects in the form of sp^3–hybridized carbons are detrimental and need to be excluded. Such structural defects are linked to, on one hand, the preparation of GNPs and, on the other, the GNP functionalization.

5. Bulk Materials

5.1. Bulk: Semiconductor Porphyrin Electrodes for Photovoltaic Photon-Conversion

Incorporation of ZnPs (**38**) and H_2Ps (**37**) into electrodes for dye-sensitized solar cell (DSSC) applications was investigated with different approaches. First, the linkage of H_2P (**37**) onto ZnO nanoparticles (NP) was analyzed—**Figure 16**.[123] The size of networks was controlled by different factors such as the ratio of H_2P to ZnO NPs, size of ZnO NPs, and aging time. These networks were probed in TiO_2- and ZnO-based DSSCs. While the fill factor (FF) remained constant, the open-circuit voltage (V_{OC}) increased from 0.57 to 0.61 V and the short circuit current (J_{SC}) increased from 5.66 to 6.78 mA cm^{-2} for the TiO_2-based DSSCs. This led to an increase in photon conversion efficiency (PCE) from 2.73% to 3.01%. These trends were additionally observed in the incident photon-to-electron conversion efficiency (IPCE). Increased stability with respect to ZnO—H_2P networks was achieved in the case of ZnO—ZnP. The latter was accompanied by a higher resistance for charge-recombination and a lower resistance towards charge-transport. Additionally, lifetime and charge-collection efficiencies increased with improved charge-injection and charge-transport in these new devices.

In a second study, catechol-functionalized ZnO nanorods were used to construct layer-by-layer (LbL) assemblies for use in solar cells.[124] The characteristic Soret- and Q-band absorptions linearly intensified for H_2P^{12-} (**39**) featuring 12 negative charges—**Figure 17**. Full coverage was obtained after three double layers of the nanorods and H_2P^{12-}s, as confirmed by SEM. Additionally, the formation of porphyrin-nanorod double-layers was substantiated by means of profilometry. A layer thicknesses of 17.6 nm for one double-layer was detected, being in line with the thickness of the nanorods with 17.0 nm. SEM images showed individual and homogenously distributed ZnO nanorods. Adjusting the basicity led to sharpening of the Soret-band absorption at 429 nm, through suppression of H-aggregate formation of the Ps. A ZnO—H_2P LbL assembly proved superior

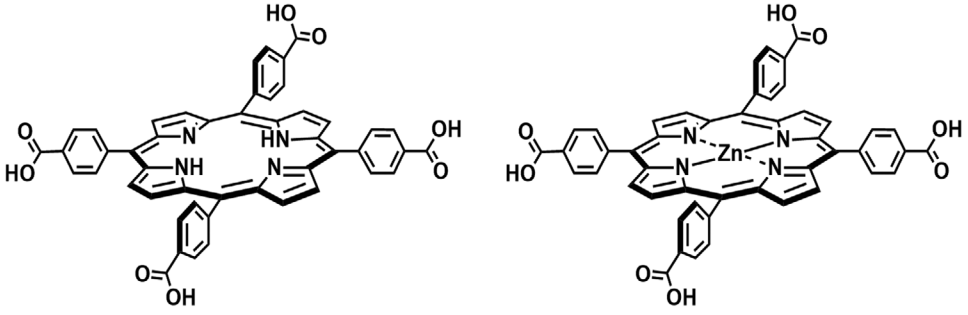

Figure 16. Representative Ps for photovoltaic photon-conversion: a light harvesting/electron donating free-base porphyrin (H_2P) (**37**) on the left and a light harvesting/electron donating zinc (II) porphyrin (ZnP) (**38**) on the right.

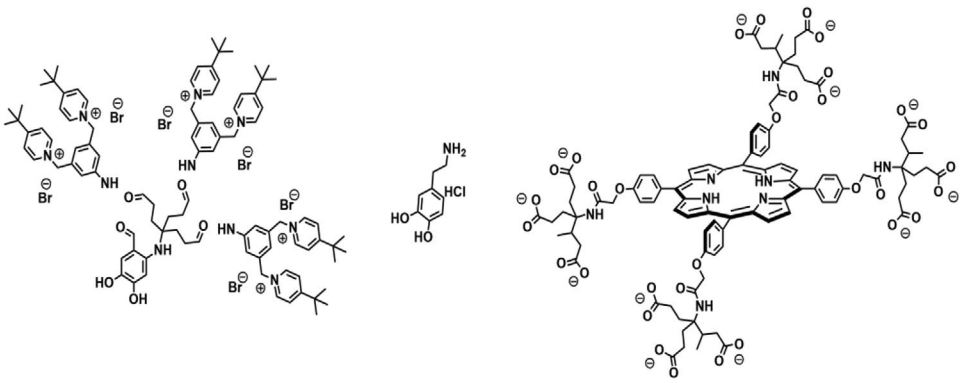

Figure 17. Representative derivatives and Ps for photovoltaic photon-conversion: a positively charged/electron accepting catechol derivative on the left, Dopamine hydrochloride in the center for the stabilization of ZnO nanorods, and a light harvesting/electron donating anionic free-base porphyrin with 12 negative charges (H_2P^{12-}) (**39**) on the right.

in current-voltage (*J-V*) and IPCE characteristics yielding a V_{OC} of 0.48 V, a J_{SC} of 0.1 mA cm^{-2}, and a PCE of 1.5×10^{-2}%, which is four times higher than the ZnO–ZnP efficiency.

5.2. Bulk: Semiconductor Porphyrin Systems for Photocatalytic Photon-Conversion

Quite different was the approach, in which porphyrin photocatalysts were developed for highly efficient photocatalytic H_2-production systems. To this end, palladium porphyrins (PdP) (**40**) and platinum porphyrins (PtP) (**41**) were utilized as photocatalysts upon their adsorption onto TiO_2 NP—**Figure 18**. A twofold role of TiO_2 NPs was the modus operandi in photo-catalytic schemes. On one hand, TiO_2 acted as a strong electron acceptor that enabled electron transfer from the porphyrin catalysts that were adsorbed onto its surface. On the other hand, TiO_2 acted as a scaffold for self-organization. To this end, the formation of J- and H-aggregates occurred on the TiO_2 surface affording photo-catalytic active schemes that power the H_2-evolution with PdP (**40**) and PtP (**41**), respectively. Overall, *J*-type conformation was more efficient than H-type conformation. Complementary time-resolved transient absorption spectroscopy helped in rationalizing that a symmetry breaking charge separation (SBCS) between individual PdPs (**40**) and PtPs (**41**) immobilized onto TiO_2 is responsible for the photocatalytic effects. Simultaneous adsorption of PdP and PtP onto TiO_2 NPs, resulted in the most efficient catalytic system illustrating 22.733 turnover numbers (TONs) and 30.200 µmol (H_2)/g (cat).[125]

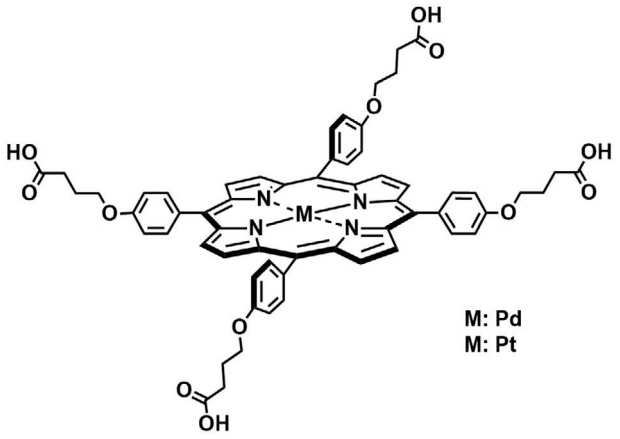

Figure 18. Representative Ps for photocatalytic photon-conversion: light harvesting/electron donating metallo(porphyrins) PdP (**40**) and PtP (**41**) immobilized on TiO_2 for H_2 production.

6. Multi-Dimensional Nanocarbons

The incorporation of 0D, 1D, and 2D nanocarbons into advanced energy materials has enabled remarkable breakthroughs in the realization of efficient energy conversion and storage units. At this stage, the grand challenge is not only to combine these nanocarbons into integrated electron donor-acceptor conjugates, but also to build on the synergy of their outstanding features in terms of photon- and charge-management. What stands out is to mix and match the electron accepting nature of 0D empty fullerenes, the electron accepting/donating nature of 0D EMFs, the electron accepting/donating nature of 1D SWCNTs, and the semi-metal nature of 2D graphene or their smaller CND and HBC analogous.[53,55,112,126–137]

6.1. 0D/0D: (Empty Fullerene)–EMF Conjugates

Given the higher stability and the lower oxidation potential of trimetallic nitride fullerenes compared to C_{60}, an all–fullerene electron donor-acceptor conjugate was designed using sequential 1,3-dipolar cycloadditions. In particular, $Lu_3N@I_h$-C_{80}, which is one of the most studied EMF, was integrated via phenyl-linker together with C_{60} —**Figure 19**. The C_{60}—$Lu_3N@I_h$-C_{80} conjugate (**42** and **43**) was the first reported example, where fullerenes behave both as electron donors and electron acceptors. DFT calculations provided evidence for the fact that the anti-RSSS isomer is the most stable out of the 16 diastereomeric pairs, that is, 8 with syn and 8 with anti-orientation. With the aid of spectroelectrochemical measurements and femtosecond transient absorption experiments, formation of a 1179 ps lived $C_{60}^{\bullet-}$—$Lu_3N@I_h$-$C_{80}^{\bullet+}$ charge-separated state was testified. The heavy-atom effect stemming from the Lu_3N-cluster facilitated the spin conversion from the charge-separated singlet state $C_{60}^{\bullet-}$—$Lu_3N@$

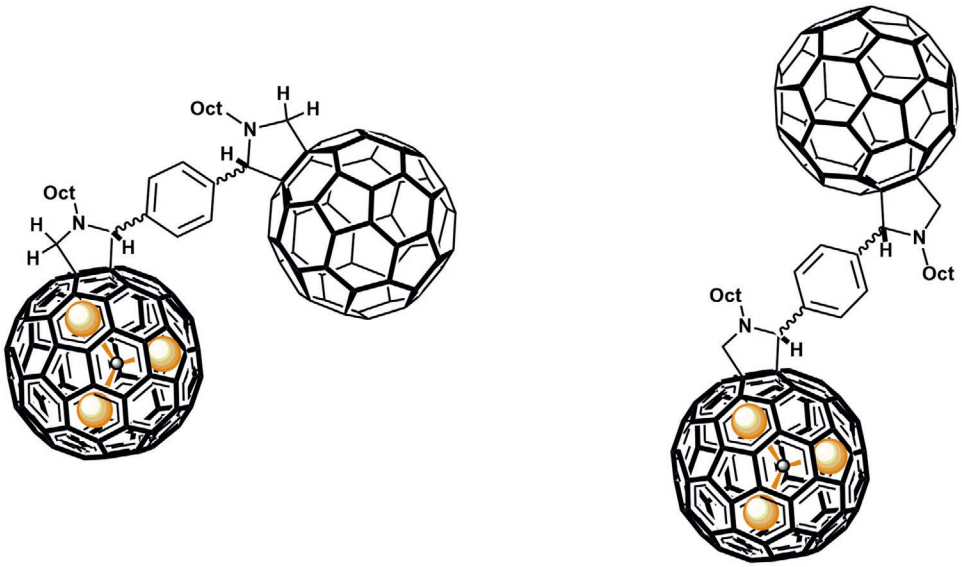

Figure 19. Representative all carbon-conjugates featuring 0D empty fullerenes and 0D EMFs: syn-C_{60}—$Lu_3N@I_h$-C_{80} stereoisomer **(42)** with an electron accepting C_{60} and electron donating $Lu_3N@I_h$-C_{80} on the left and anti-C_{60}—$Lu_3N@I_h$-C_{80} stereoisomer **(43)** with an electron accepting C_{60} and electron donating $Lu_3N@I_h$-C_{80} on the right. In anisole, the CS and recombination are 1.83×10^{11} and 8.5×10^8 s^{-1} (singlet charge-separated state)/1.18×10^8 s^{-1} (triplet charge-separated state), respectively.

I_h-$C_{80}^{\bullet+}$ into the corresponding triplet state. This, in turn, slowed down the CR by one order of magnitude.[138]

6.2. 0D/1D: (Empty Fullerene)–SWCNT Conjugates and EMF–SWCNT Conjugates

Recently, C_{60} and EMFs, on one hand, and SWCNTs, on the other hand, were merged into covalent conjugates. Herein, three different conjugates of C_{60} with SWCNTs (**44–46**) as well as one conjugate of EMF with SWCNTs are highlighted—**Figure 20**. In the case of C_{60}—SWCNT (**44**), Raman spectroscopy was used to verify the covalent attachment.[139] The I_D/I_G ratio for C_{60}—SWCNT (0.96) was greater than that seen in pristine SWCNTs (0.43). In addition, the presence of up-shifts in the G- and D-modes and down-shift in the $A_g(2)$-mode was interpreted in terms of a charge-transfer, which takes place from SWCNTs to C_{60} as a result of the strong electron-accepting nature of C_{60}.

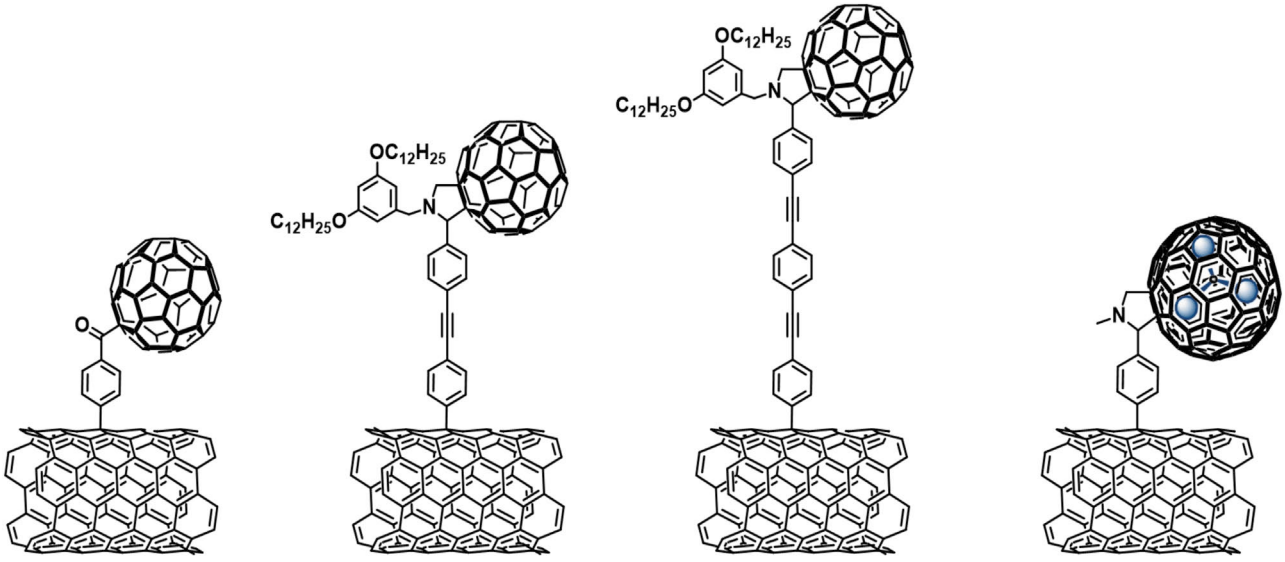

Figure 20. Representative all carbon-conjugates featuring 0D empty fullerenes/EMFs and 1D SWCNTs: C_{60}—SWCNT (**44**) with an electron donating SWCNT and an electron accepting C_{60} on the left, C_{60}—SWCNT (**45**) with an electron donating SWCNT and an electron accepting C_{60} in the center left, C_{60}—SWCNT (**46**) with an electron donating SWCNT and an electron accepting C_{60} in the center right, and $Sc_3N@C_{80}$—SWCNT (**47**) (Sc_3N^{6+} is shown in blue) with an electron donating SWCNT and an electron accepting $Sc_3N@C_{80}$ on the right. In DMF, CS is 2.0×10^{11} s^{-1} (C_{60}—SWCNT (**45**))/$\geq 2.0 \times 10^{11}$ s^{-1} (C_{60}—SWCNT (**46**)).

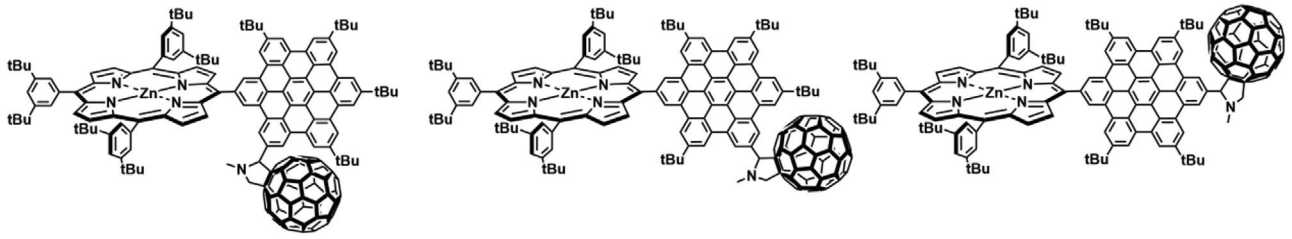

Figure 21. Representative porphyrin conjugates featuring 2D HBC and 0D C_{60}: ortho-(C_{60}—HBC—ZnP) (**48**) with a light harvesting/electron donating ZnP, electron transfer mediating HBC, and an electron accepting C_{60} on the left meta-(C_{60}—HBC—ZnP) (**49**) with a light harvesting/electron donating ZnP, electron transfer mediating HBC, and an electron accepting C_{60} in the center, and para-(C_{60}—HBC—ZnP) (**50**) with a light harvesting/electron donating ZnP, electron transfer mediating HBC and an electron accepting C_{60} on the right.

In an independent study, C_{60} and SWCNT were covalently linked using phenylene-ethylene bridges to control electronic communication and to vary the C_{60}-to-SWCNT distance.[140] The broadened absorptions in the visible range in the case of C_{60}—SWCNT (**45**) and C_{60}—SWCNT (**46**) was used as a sign for the functionalization, on one hand, and the electronic interaction between C_{60} and SWCNT, on the other hand. In addition, a significantly more intense D-band for C_{60}—SWCNT (**45**) and C_{60}—SWCNT (**46**) resulted in remarkably higher I_D/I_G ratios of 0.35 and 0.62, respectively, when compared to that of just SWCNTs (0.07). This was due to the addition of the aryls onto the SWCNT skeleton. Femtosecond transient absorption studies shed light onto the charge-separation and charge-recombination events. The transient maxima for C_{60}—SWCNT (**45**) were red-shifted relative to pristine SWCNTs. Moreover, from a faster-excited state recovery compared to pristine SWCNTs an additional deactivation process, that is, electron transfer from in situ formed SWCNT exciton to C_{60}, was inferred. The recovery process was fully completed within nearly 5 ps. Similar performances were summarized for C_{60}—SWCNT (**46**). But, the underlying red-shift was much smaller, and the excited state recovery was slower than that observed for C_{60}—SWCNT (**45**). As such, in C_{60}—SWCNT (**46**) the larger C_{60} to SWCNT distance went hand-in-hand with a much slower charge-separation.

Next, the focus was set on a $Sc_3N@C_{80}$—SWCNT conjugate (**47**).[141] Here, the efficient binding of $Sc_3N@C_{80}$ to SWCNTs was realized by using negatively charged SWCNTs. Importantly, EMFs were activated by introducing diazonium functionalities, which served as SWCNT anchors. The activation of SWCNTs was accomplished through a preceding reduction with potassium. An immediate consequence is SWCNT-centered absorptions, which are blue-shifted and altered in relative intensities with respect to the pristine SWCNTs. Raman spectroscopy exposed a significantly more intense D-band in the case of SWCNT-$Sc_3N@C_{80}$ with a much higher I_D/I_G ratio (0.37) compared with pristine SWCNTs. The Raman mode at 411 cm^{-1} in SWCNT-$Sc_3N@C_{80}$ was slightly up-shifted relative to $Sc_3N@C_{80}$, implying intramolecular interactions between $Sc_3N@C_{80}$ and SWCNT in the conjugate.

6.3. 0D/2D: (Empty Fullerene)–HBC Conjugates

Of further interest was HBCs, which acted as bridges between C_{60} and ZnP. Notably, HBCs were used as a versatile platform to create ortho-, meta-, and para-isomeric substitution patterns (**48 – 50**)—**Figure 21**. Compared to a C_{60}—HBC reference, the HBC-related absorptions were broadened in ortho-(C_{60}—HBC—ZnP) (**48**), meta-(C_{60}—HBC—ZnP) (**49**), and para-(C_{60}—HBC—ZnP) (**50**). In preliminary transient absorption experiments, the fast formation of a charge-transfer state is observed followed by the transformation into a singlet charge-separated state $C_{60}^{\bullet-}$—HBC—$ZnP^{\bullet+}$, which eventually ends up in a triplet charge-separated state. The charge-recombination

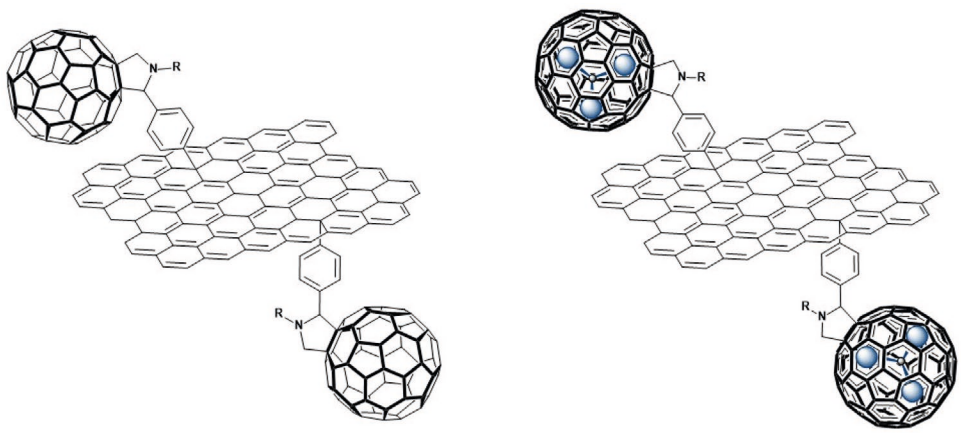

Figure 22. Representative all carbon-conjugates featuring 0D empty fullerenes/EMFs and 2D GNPs: C_{60}—GNP (**51**) with an electron accepting C_{60} and electron donating GNP on the left and $Sc_3N@I_h$-C_{80}—GNP (**52**) with an electron accepting GNP and electron donating $Sc_3N@I_h$-C_{80}. on the right.

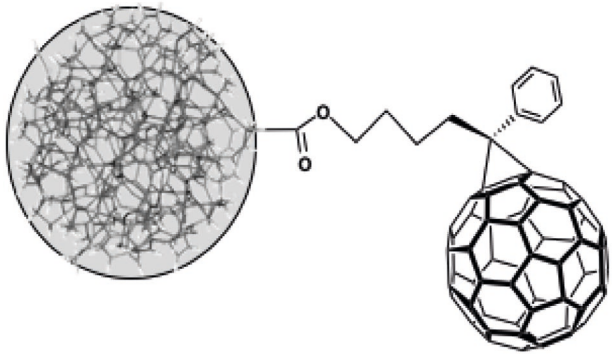

Figure 23. Representative all carbon-conjugate featuring 0D empty fullerenes and 2D CNDs: C_{60}—CND (**53**) with an electron accepting C_{60} and electron donating CND. This system is currently under investigation.

was strongly solvent-dependent and ranged from nanoseconds in nonpolar media to hundreds of picoseconds in polar media. Another interesting aspect evolved in ortho-(C_{60}—HBC—ZnP) (**48**). Here, the formation of the charge-transfer and charge-separation is accelerated due to the proximity of C_{60} and ZnP, enabling an alternative through-space pathway next to the through-bond pathway, which was also monitored in meta-(C_{60}—HBC—ZnP) (**49**) and para-(C_{60}—HBC—ZnP) (**50**).[142]

6.4. 0D/2D: (Empty Fullerene)–GNP and EMF–GNP Conjugates

The covalent functionalization of graphene continues to constitute a tremendous task and this motivated the synthesis of inter carbon-allotrope architectures based on graphene—**Figure 22**. Rather than using oxidized sheets of graphene, the focus was on the functionalization of pristine graphene in the form of GNPs, specifically with 0D empty fullerenes and EMFs. To this end, grafting GNPs with C_{60} and $Sc_3N@I_h$-C_{80} was realized using a reductive activation/exfoliation pathway of graphite. To settle the nature of the binding C_{60}—GNP (**51**) and $Sc_3N@I_h$-C_{80}—GNP (**52**) were characterized by mass spectroscopy. Additionally, statistical Raman spectroscopy assisted in the confirmation by means of considerably more intense D-bands in the C_{60}—GNP (**51**) and $Sc_3N@I_h$-C_{80}—GNP conjugates (**52**) when compared to the starting material, that is, pristine graphene. For example, I_D/I_G ratio is 1.2 higher compared with ca. 0.1 for graphite.[143,144]

6.5. 0D/2D: (Empty Fullerene)–CND Conjugates

Lately, the first examples of C_{60}—CND conjugates (**53**) were prepared and are being actively investigated—**Figure 23**. In preliminary experiments, substantial quenching of the CND-centered emission suggested that electronic communication between CNDs and C_{60} enabled new decay pathways that were absent in the individual components. This was interpreted in terms of energy or electron transfer between the components, that is, C_{60} and CND.[145]

Recent years have witnessed a trend-setting for combining the best of the 0D, 1D, and 2D nanocarbons—**Scheme 5**. Early work has truly been promising and provided important incentives to optimize the design, synthesis, and study of advanced energy materials.

7. Conclusion

Years of trend-setting research in the area of 0D, 1D, and 2D nanocarbons has witnessed notable breakthroughs in advanced

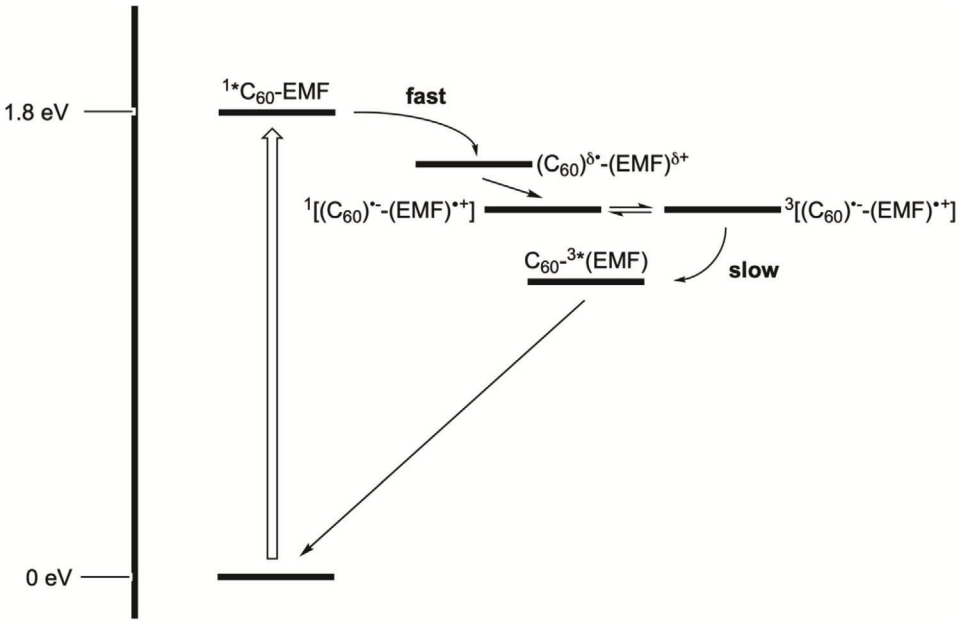

Scheme 5. Energy diagram for empty fullerene EMF conjugates highlighting the fast CS and slow CR stemming from the heavy atom affect in EMFs to spin-flip the charge separated state.

Table 1. CS and CR rate constants determined for the different conjugates featuring 0D, 1D, and 2D nanocarbons, on one hand, and MPs, on the other hand, from the pump-probe femtosecond measurements at an excitation wavelength relevant to the studied systems in solvents of different polarities.

	Conjugate	Solvent	k_{CS} [s^{-1}]	k_{CR} [s^{-1}]	Ref.
1	C_{60}—ZnP	THF	$>2.9 \times 10^{11}$	2.5×10^{9}	[71]
4	C_{60}—CoP	THF	5.5×10^{10}	4.3×10^{9}	[72]
7	C_{60}—ZnP	THF	1.3×10^{10} 5.1×10^{8} 1.6×10^{7}	3×10^{5}	[73]
11	C_{60}—(o*p*PV)$_3$—ZnP	THF	4.5×10^{9}	1.2×10^{6}	[74]
12	C_{60}—(Co*p*PV)$_3$—ZnP	THF	7.1×10^{10}	5.9×10^{9}	[75]
13	C_{60}—H_2P	benzonitrile	1.8×10^{11}	3.4×10^{9}	[76–78]
14	C_{60}—ZnP	benzonitrile	4.8×10^{11}	2.0×10^{10}	[76–78]
15	$Ce_2@I_h$-C_{80}—ZnP	THF	1.3×10^{12}	2.4×10^{8}	[86]
16	$Ce_2@I_h$-C_{80}—H_2P	THF	5.4×10^{10}	$>5.4 \times 10^{10}$	[87]
17	$La_2@I_h$-C_{80}—ZnP	THF	1.0×10^{12}	5.8×10^{9}	[88]
18	$Sc_3N@I_h$-C_{80}—ZnP	toluene	1.0×10^{11}	2.3×10^{10}	
19	$Sc_3N@I_h$-C_{80}—ZnP	THF	$>1 \times 10^{12}$	1.0×10^{6}	[89]
20	$Sc_3N@I_h$-C_{80}—ZnP	THF	$>1 \times 10^{12}$	6.6×10^{5}	[89]
21	SWCNT—ZnP	THF	$>1 \times 10^{12}$	2.0×10^{11}	[95]
22	SWCNT—ZnP	DMF	$>1 \times 10^{12}$	4.2×10^{10}	[96]
23	SWCNT—ZnP	DMF	$>1 \times 10^{12}$	2.0×10^{10}	[96]
24	SWCNT—(H_2P)$_4$	THF	1.5×10^{10}	2.9×10^{6}	[97]
25	SWCNT—H_2P	THF	$>1 \times 10^{12}$	2.0×10^{10}	[98]
26	SWCNT—ZnP	DMF	$>1 \times 10^{12}$	1.2×10^{9}	[99]
27	SWCNT—(ZnP)$_2$	DMF	$>1 \times 10^{12}$	5.0×10^{9}	[99]
28	CND-H_2P	H_2O/THF 1:1	$>1 \times 10^{12}$	1.59×10^{11} 4.44×10^{9}	[115]
34	(HBC—ZnP—ZnP—HBC)—C_{60}	chlorobenzene	$0.25–1.25 \times 10^{12}$	$1.05–2.63 \times 10^{9}$	[117]
35	Fc-(*p*-phenyleneethynylene)$_2$—ZnP-(*p*-phenyleneethynylene)$_2$—GNP	THF	Fc^{+}—ZnP^{-}—GNP 1.8×10^{11}	Fc—ZnP^{+}—GNP^{-} 9.88×10^{10} Fc^{+}—ZnP^{-}—GNP 4.50×10^{10} Fc—ZnP^{+}—GNP^{-}/Fc^{+}—ZnP—GNP^{-} 5.50×10^{8}/$< 10^{8}$	[120–122]
36	Fc—(*p*-phenyleneethynylene)$_2$—ZnP-(*p*-phenyleneethynylene)$_2$—GNP	THF	Fc^{+}—ZnP^{-}—GNP 1.60×10^{10}	Fc—ZnP^{+}—GNP^{-} 7.20×10^{10} Fc^{+}—ZnP^{-}—GNP 5.0×10^{9} Fc—ZnP^{+}—GNP^{-}/Fc^{+}—ZnP—GNP^{-} 3.87×10^{8}/$< 10^{8}$	[120–122]
42	anti-C_{60}—$Lu_3N@I_h$-C_{80}	anisole	1.83×10^{11}	8.5×10^{8} 1.18×10^{8}	[138]
45	C_{60}—SWCNT	DMF	2.0×10^{11}	$\approx 1 \times 10^{9}$	[140]

energy materials. At the forefront of efficient energy conversion and storage units has been the electron accepting nature of 0D empty fullerenes, the electron accepting/donating nature of 0D EMFs, the electron donating nature of 1D SWCNTs, and the semi-metal nature of 2D GNPs or their smaller CND and HBC analogous. In **Table 1** the most relevant rate constants are summarized. But, exploiting their full potential has required a transdisciplinary methodology. Our transdisciplinarity in the area of photon- and charge-management has always been based on the synergy stemming from synthetic chemistry, characterization, theory, and modeling as well as prototype devices. But, a prototype is merely the proof of concept, it isn't the proof of a product. To go from a prototype, which has enabled testing the idea/the general design and proving that it is possible to apply those ideas, all the way to production, and taking a prototype to a place, where it can be commercialized, takes a lot of effort, planning, and expertise.

Progress has gone much beyond advanced concepts to convert sunlight and to store energy by means of photovoltaics and H_2-photocatalysis. Decisive have been contributions/applications in molecular electronics, biomedical devices, nanocomposites, sensing, just to name a few.

From our own perspective, future challenges in the area will include the utilization of nearly defect-free and individualized/stabilized 1D SWCNTs and 2D GNPs to decorate them with suitable light harvesters, electron donors, or electron acceptors.

This will be part of the concept to foster, on one hand, the storage of single charges and, on the other hand, the accumulation of multiple charges, that is, either electrons or holes, in extended 1D SWCNTs/2D GNPs or the unidirectional mediation thereof to catalytic centers. All of this will be needed to drive, for example, the formation of solar fuel. The mediation of charges to catalytic centers will involve solving yet another challenge: Multifunctional 1D SWCNTs/2D GNPs, which feature light harvesters/electron donors and electron acceptors, but arbitrarily on both sides of the basal plane of 2D GNP. In the long run, decorating, for instance, the upper side of the 2D GNP basal plane with light harvesters/electron donors and the lower side with electron acceptors or vice versa will be the penultimate challenge in the area as it will enable storing not only single but also multiple charges, which are separated by the basal plane of 2D GNP.

Acknowledgements

This work was financially supported by the Deutsche Forschungsgemeinschaft (DFG) by the SFB953 "Synthetic Carbon Allotropes".

Open access funding enabled and organized by Projekt DEAL.

Conflict of Interest

The authors declare no conflict of interest.

Keywords

charge management, nanocarbons, photon management, solar-energy conversion

Received: September 4, 2020
Revised: October 23, 2020
Published online:

[1] J. Deisenhofer, J. R. Norris, *The Photosynthetic Reaction Center*, 1st ed., Academic Press, San Diego, USA **1993**.
[2] A. F. Collings, C. Critchley, *Artificial Photosynthesis: From Basic Biology to Industrial Application*, Wiley-VCH, Weinheim, Germany **2005**.
[3] V. Balzani, *Electron Transfer in Chemistry*, Vol. *1*, Wiley-VCH, Weinheim, Germany **2001**.
[4] M. R. Wasielewski, *Chem. Rev.* **1992**, *92*, 435.
[5] D. Gust, T. A. Moore, A. L. Moore, *Acc. Chem. Res.* **1993**, *26*, 198.
[6] S. L. Mattes, S. Farid, *Science* **1984**, *226*, 917.
[7] H. D. Roth, *A Brief History of Photoinduced Electron Transfer and Related Reactions in Photoinduced Electron Transfer*, Vol. *156* (Ed. J. Mattay), Springer, Berlin, Germany **1990**, Ch. 1.
[8] R. A. Marcus, *Angew. Chem., Int. Ed.* **1993**, *32*, 1111.
[9] T. Akasaka, S. Nagase, *A New Family of Carbon Clusters*, 1st ed., Kluwer Academic Publishers, Dordrecht, Netherland **2002**.
[10] M. S. Dresselhaus, G. Dresselhaus, P. Avouris, *Carbon Nanotubes: Synthesis, Structure, Properties and Applications*, 1st ed., Springer-Verlag, Berlin, Germany **2001**.
[11] S. Y. Y. Lim, W. Shen, Z. Gao, *Chem. Soc. Rev.* **2015**, *44*, 362.
[12] C. Zhang, Y. Liu, X. Q. Xiong, L. H. Peng, L. Gan, C. F. Chen, H. B. Xu, *Org. Lett.* **2012**, *14*, 5912.
[13] K. S. Novoselov, A. K. Geim, S. V. Morozov, D. Jiang, Y. Zhang, S. V. Dubonos, I. V. Grigorieva, A. A. Firsov, *Science* **2004**, *306*, 666.
[14] K. M. Kadish, K. Smith, R. Guillard, *Handbook of Porphyrin Science*,Vol. *10*, World Scientific Press, Singapore **2010**.
[15] H. Imahori, Y. Sakata, *Adv. Mater.* **1997**, *9*, 537.
[16] M. Prato, *J. Mater. Chem.* **1997**, *7*, 1097.
[17] N. Martin, L. Sanchez, B. Illescas, I. Perez, *Chem. Rev.* **1998**, *98*, 2527.
[18] H. Imahori, Y. Sakata, *Eur. J. Org. Chem.* **1999**, *10*, 2445.
[19] C. A. Reed, R. D. Bolskar, *Chem. Rev.* **2000**, *100*, 1075.
[20] D. Gust, T. A. Moore, A. L. Moore, *J. Photochem. Photobiol., B* **2000**, *58*, 63.
[21] D. Gust, T. A. Moore, A. L. Moore, *Acc. Chem. Res.* **2001**, *34*, 40.
[22] H. Imahori, Y. Mori, Y. Matano, *J. Photochem. Photobiol., C* **2003**, *4*, 51.
[23] J. F. Nierengarten, *Top. Curr. Chem.* **2003**, *228*, 87.
[24] M. E. El-Khouly, O. Ito, F. D'Souza, *J. Photochem. Photobiol., C* **2004**, *5*, 79.
[25] J. Wu, W. Pisula, K. Müllen, *Chem. Rev.* **2007**, *107*, 718.
[26] A. Cadranel, J. T. Margraf, V. Strauss, T. Clark, D. M. Guldi, *Acc. Chem. Res.* **2019**, *52*, 955.
[27] J. D. Megiatto, D. I. Schuster, G. de Miguel, S. Wolfrum, D. M. Guldi, *Chem. Mater.* **2012**, *24*, 2472.
[28] C. Rosso, G. Filippini, M. Prato, *ACS Catal.* **2020**, *10*, 8090.
[29] S. Zhuo, M. Shao, S.-T. Lee, *ACS Nano* **2012**, *6*, 1059.
[30] H. Luo, Q. Guo, P. A. Szilagyi, A. B. Jorge, M. M. Titirici, *Trends Chem.* **2020**, *2*, 623.
[31] W. Meng, X. Bai, B. Wang, Z. Liu, S. Lu, B. Yang, *Energy Environ. Mater.* **2019**, *2*, 172.
[32] M. M. Al Mogren, N. M. Ahmed, A. A. Hasanein, *J. Saudi Chem. Soc.* **2020**, *24*, 303.
[33] J. M. Park, J. H. Lee, W. -D. Jang, *Coord. Chem. Rev.* **2020**, *407*, 213157.
[34] M. Joseph, S. Haridas, *Int. J. Hydrog. Energy* **2020**, *45*, 11954.
[35] G. d. A. M. Safar, D. C. d. S. Martins, G. D. Silva, J. S. Reboucas, Y. M. Idemori, A. Righi, *Synth. Met.* **2014**, *193*, 64.
[36] I. R. Tagle, W. Orellana, *Phys. Rev. B* **2010**, *82*, 115406.
[37] M. Zhu, J. Chen, L. Huang, R. Ye, J. Xu, Y. -F. Han, *Angew. Chem., Int. Ed.* **2019**, *58*, 6595.
[38] A. Wang, J. Song, Z. Huang, Y. Song, W. Yu, H. Dong, W. Hu, M. P. Cifuentes, M. G. Humphrey, L. Zhang, J. Shao, C. Zhang, *Nano Res.* **2016**, *9*, 458.
[39] I. Hijazi, T. Bourgeteau, R. Cornut, A. Morozan, A. Filoramo, J. Leroy, V. Derycke, B. Jousselme, S. Campidelli, *J. Am. Chem. Soc.* **2014**, *136*, 6348.
[40] L. Meng, C. Fu, Q. Lu, *Prog. Nat. Sci.* **2009**, *19*, 801.
[41] V. T. Veetil, G. Prabhavathi, R. Yamuna, *IOP Conf. Ser.: Mater. Sci. Eng.* **2019**, *577*, 012091.
[42] A. Wang, Y. Fang, L. Long, Y. Song, W. Yu, W. Zhao, M. P. Cifuentes, M. G. Humphrey, C. Zhang, *Chem. - Eur. J.* **2013**, *19*, 14159.
[43] G. Prabhavathi, R. Yamuna, A. C. Jafer, *J. Organomet. Chem.* **2018**, *861*, 219.
[44] S. Kirner, M. Sekita, D. M. Guldi, *Adv. Mater.* **2014**, *26*, 1482.
[45] A. Zieleniewska, F. Lodermeyer, A. Roth, D. M. Guldi, *Chem. Soc. Rev.* **2018**, *47*, 702.
[46] D. Dasler, R. A. Schäfer, M. B. Minameyer, J. F. Hitzenberger, F. Hauke, T. Drewello, A. Hirsch, *J. Am. Chem. Soc.* **2017**, *139*, 11760.
[47] M. Vizuete, M. Barrejón, M. J. Gómez-Escalonilla, F. Langa, *Nanoscale* **2012**, *4*, 4370.
[48] M. Chen, R. Guan, S. Yang, *Adv. Sci.* **2019**, *6*, 1800941.
[49] V. Nikolaou, A. Charisiadis, C. Stangel, G. Charalambidis, A. G. Coutsolelos, *C* **2019**, *5*, 57.
[50] L. Basurto, F. Amerikheirabadi, R. Zope, T. Baruah, *Phys. Chem. Chem. Phys.* **2015**, *17*, 5832.
[51] A. Narita, X.-Y. Wang, X. Feng, K. Müllen, *Chem. Soc. Rev.* **2015**, *44*, 6616.
[52] D. Lu, G. Zhuang, H. Wu, S. Wang, S. Yang, P. Du, *Angew. Chem., Int. Ed.* **2017**, *56*, 158.

[53] Y. Hu, L. F. Dössel, X.-Y. Wang, S. Mahesh, W. Pisula, S. De Feyter, X. Feng, K. Müllen, A. Narita, *ChemPlusChem* **2017**, *82*, 1030.
[54] H. Seyler, B. Purushothaman, D. J. Jones, A. B. Holmes, W. W. H. Wong, *Pure Appl. Chem.* **2012**, *84*, 1047.
[55] W. W. H. Wong, T. Khoury, D. Vak, C. Yan, D. J. Jones, M. J. Crossley, A. B. Holmes, *J. Mater. Chem.* **2010**, *20*, 7005.
[56] A. B. S. Elliott, R. Horvath, X.-Z. Sun, M. G. Gardiner, K. Müllen, N. T. Lucas, M. W. George, K. C. Gordon, *Inorg. Chem.* **2016**, *55*, 4710.
[57] S. M. Draper, D. J. Gregg, E. R. Schofield, W. R. Browne, M. Duati, J. G. Vos, P. Passaniti, *J. Am. Chem. Soc.* **2004**, *126*, 8694.
[58] H. H. Dam, K. Sun, E. Hanssen, J. M. White, T. Marszalek, W. Pisula, J. Czolk, J. Ludwig, A. Colsmann, M. Pfaff, D. Gerthsen, W. W. H. Wong, D. J. Jones, *ACS Appl. Mater. Interfaces* **2014**, *6*, 8824.
[59] D. Reger, P. Haines, F. W. Heinemann, D. M. Guldi, N. Jux, *Angew. Chem., Int. Ed.* **2018**, *57*, 5938.
[60] P. A. Liddell, J. P. Sumida, A. N. MacPherson, L. Noss, G. R. Seely, K. N. Clark, A. L. Moore, T. A. Moore, D. Gust, *Photochem. Photobiol.* **1994**, *60*, 537.
[61] D. M. Guldi, *Chem. Soc. Rev.* **2002**, *31*, 22.
[62] D. M. Guldi, G. M. A. Rahman, C. Ehli, V. Sgobba, *Chem. Soc. Rev.* **2006**, *35*, 471.
[63] V. Sgobba, D. M. Guldi, *Chem. Soc. Rev.* **2009**, *38*, 165.
[64] M. Rudolf, S. V. Kirner, D. M. Guldi, *Chem. Soc. Rev.* **2016**, *45*, 612.
[65] G. Bottari, M. A. Herranz, L. Wibmer, M. Volland, L. Rodriguez-Perez, D. M. Guldi, A. Hirsch, N. Martin, F. D'Souza, T. Torres, *Chem. Soc. Rev.* **2017**, *46*, 4464.
[66] A. Hirsch, *Fullerenes and Related Structures*, 1st ed., Springer, Berlin, Germany **1999**.
[67] H. Imahori, H. Yamada, D. M. Guldi, Y. Endo, A. Shimomura, S. Kundu, K. Yamada, T. Okada, Y. Sakata, S. Fukuzumi, *Angew. Chem., Int. Ed.* **2002**, *41*, 2344.
[68] S. Fukuzumi, K. Ohkubo, H. Imahori, D. M. Guldi, *Chem. - Eur. J.* **2003**, *9*, 1585.
[69] X. Lu, L. Echegoyen, A. L. Balch, S. Nagase, T. Akasaka, *Endohedral Metallofullerenes: Basics and Applications*, 1st ed., CRC Press, Florida, USA **2014**.
[70] A. Popov, S. Yang, L. Dunsch, *Chem. Rev.* **2013**, *113*, 5989.
[71] D. M. Guldi, C. Luo, M. Prato, E. Dietel, A. Hirsch, *Chem. Commun.* **2000**, 373.
[72] L. R. Sutton, M. Scheloske, K. S. Pirner, A. Hirsch, D. M. Guldi, J.-P. Gisselbrecht, *J. Am. Chem. Soc.* **2004**, *126*, 10370.
[73] H. Imahori, K. Tamaki, D. M. Guldi, C. Luo, M. Fujitsuka, O. Ito, Y. Sakata, S. Fukuzumi, *J. Am. Chem. Soc.* **2001**, *123*, 2607.
[74] C. Schubert, J. T. Margraf, T. Clark, D. M. Guldi, *Chem. Soc. Rev.* **2015**, *44*, 988.
[75] J. Sukegawa, C. Schubert, X. Z. Zhu, H. Tsuji, D. M. Guldi, E. Nakamura, *Nat. Chem.* **2014**, *6*, 899.
[76] T. Drovetskaya, C. A. Reed, P. D. W. Boyd, *Tetrahedron Lett.* **1995**, *36*, 7971.
[77] D. Kuciauskas, S. Lin, G. R. Seely, A. L. Moore, T. A. Moore, D. Gust, T. Drovetskaya, C. A. Reed, P. D. W. Boyd, *J. Phys. Chem.* **1996**, *100*, 15926.
[78] D. Gust, T. A. Moore, A. L. Moore, *Res. Chem. Intermed.* **1997**, *23*, 621.
[79] D. Gust, T. A. Moore, A. L. Moore, *Acc. Chem. Res.* **2009**, *42*, 1890.
[80] P. D. W. Boyd, C. A. Reed, *Acc. Chem. Res.* **2005**, *38*, 235.
[81] F. D'Souza, O. Ito, *Chem. Comm.* **2009**, 4913.
[82] H. Imahori, S. Fukuzumi, *Adv. Funct. Mater.* **2004**, *14*, 525.
[83] T. Hasobe, *Phys. Chem. Chem. Phys.* **2010**, *12*, 44.
[84] H. Imahori, *Bull. Chem. Soc. Jpn.* **2007**, *80*, 621.
[85] M. Rudolf, O. Trukhina, J. Perles, L. Feng, T. Akasaka, T. Torres, D. M. Guldi, *Chem. Sci.* **2015**, *6*, 4141.
[86] D. M. Guldi, L. Feng, S. G. Radhakrishnan, H. Nikawa, M. Yamada, N. Mizorogi, T. Tsuchiya, T. Akasaka, S. Nagase, M. A. Herranz, N. Martín, *J. Am. Chem. Soc.* **2010**, *132*, 9078.
[87] M. Rudolf, L. Feng, Z. Slanina, W. Wang, S. Nagase, T. Akasaka, D. M. Guldi, *Nanoscale* **2016**, *8*, 13257.
[88] L. Feng, S. G. Radhakrishnan, N. Mizorogi, Z. Slanina, H. Nikawa, T. Tsuchiya, T. Akaksaka, S. Nagase, M. Martín, D. M. Guldi, *J. Am. Chem. Soc.* **2011**, *133*, 7608.
[89] S. Wolfrum, J. R. Pinzon, A. Molina-Ontario, A. Gouloumis, N. Martín, L. Echegoyen, D. M. Guldi, *Chem. Commun.* **2011**, *47*, 2270.
[90] F. Langa, M. J. Gomez-Escalonilla, P. de la Cruz, *J. Porphyrins Phthalocyanines* **2007**, *11*, 348.
[91] A. Wang, J. Ye, M. G. Humphrey, C. Zhang, *Adv. Mater.* **2018**, *30*, 1705704.
[92] D. Baskaran, J. W. Mays, X. P. Zhang, M. S. Bratcher, *J. Am. Chem. Soc.* **2005**, *127*, 6916.
[93] I. Hijazi, K. Khedhiri, S. Campidelli, *Org. Biomol. Chem.* **2018**, *16*, 6767.
[94] A. Staicu, A. Pascu, V. Nastasa, M. L. Pascu, *Rom. Rep. Phys.* **2015**, *67*, 1457.
[95] L. M. Arellano, M. Barrejon, H. B. Gobeze, M. J. Gomez-Escalonilla, J. L. G. Fierro, F. D'Souza, F. Langa, *Nanoscale* **2017**, *9*, 7551.
[96] J. Baek, T. Umeyama, S. Mizuno, N. V. Tkachenko, H. Imahori, *J. Phys. Chem. C.* **2018**, *122*, 13285.
[97] S. Campidelli, C. Sooambar, E. L. Diz, C. Ehli, D. M. Guldi, *J. Am. Chem. Soc.* **2006**, *128*, 12544.
[98] C. Ehli, S. Campidelli, F. G. Brunetti, M. Prato, D. M. Guldi, *J. Porphyrins Phthalocyanines* **2007**, *11*, 442.
[99] T. Palacin, H. L. Khanh, B. Jousselme, P. Jegou, A. Filoramo, C. Ehli, D. M. Guldi, S. Campidelli, *J. Am. Chem. Soc.* **2009**, *131*, 15394.
[100] B. Girek, W. Sliwa, *J. Inclusion Phenom. Macrocyclic Chem.* **2015**, *82*, 283.
[101] S. Supriya, V. S. Shetti, G. Hegde, *New J. Chem.* **2018**, *42*, 12328.
[102] Z. Guo, F. Du, D. Ren, Y. Chen, J. Zheng, Z. Liu, J. Tian, *J. Mater. Chem.* **2006**, *16*, 3021.
[103] S. P. Economopoulos, A. Skondra, K. Ladomenou, N. Karousis, G. Charalambidis, A. G. Coutsolelos, N. Tagmatarchis, *RSC Adv.* **2013**, *3*, 5539.
[104] H. Li, Z. Kang, Y. Liu, S. -T. Lee, *J. Mater. Chem.* **2012**, *22*, 24230.
[105] Z. Li, L. Wang, Y. Li, Y. Feng, W. Feng, *Mater. Chem. Front.* **2019**, *3*, 2571.
[106] M. L. Liu, B. B. Chen, C. M. Li, C. Z. Huang, *Green Chem.* **2019**, *21*, 449.
[107] C. M. Carbonaro, R. Corpino, M. Salis, F. Mocci, S. V. Thakkar, C. Olla, P. C. Ricci, *C* **2019**, *5*, 60.
[108] A. Sciortino, A. Cannizzo, F. Messina, *C* **2018**, *4*, 67.
[109] B. De, N. Karak, *J. Mater. Chem. A* **2017**, *5*, 1826.
[110] H. Yu, R. Shi, Y. Zhao, G. I. N. Waterhouse, L. -Z. Wu, C. -H. Tung, T. Zhang, *Adv. Mater.* **2016**, *28*, 9454.
[111] R. Rieger, K. Müllen, *J. Phys. Org. Chem.* **2010**, *23*, 315.
[112] V. Strauss, A. Roth, M. Sekita, D. M. Guldi, *Chem* **2016**, *1*, 531.
[113] M. Yi, Z. Shen, *J. Mater. Chem. A* **2015**, *3*, 11700.
[114] L. Pierantoni, D. Mencarelli, M. Bozzi, R. Moro, S. Moscato, L. Perregrini, F. Micciulla, A. Cataldo, S. Bellucci, *IEEE Trans. Microwave Theory Tech.* **2015**, *63*, 2491.
[115] F. Arcudi, V. Strauss, L. Dordevic, A. Cadranel, D. M. Guldi, M. Prato, *Angew. Chem., Int. Ed.* **2017**, *56*, 12097.
[116] M. M. Martin, D. Lungerich, P. Haines, F. Hampel, N. Jux, *Angew. Chem., Int. Ed.* **2019**, *58*, 8932.
[117] M. Wolf, D. Lungerich, S. Bauroth, M. Popp, B. Platzer, T. Clark, H. L. Anderson, N. Jux, D. M. Guldi, *Chem. Sci.* **2020**, *11*, 7123.
[118] V. Georgakilas, M. Otyepka, A. B. Bourlinos, V. Chandra, N. Kim, K. C. Kemp, P. Hobza, R. Zboril, K. S. Kim, *Chem. Rev.* **2012**, *112*, 6156.
[119] A. Stergiou, G. Pagona, N. Tagmatarchis, *J. Nanotechnol.* **2014**, *5*, 1580.

[120] F. Possanza, F. Limosani, P. Tagliatesta, R. Zanoni, M. Scarselli, E. Ciotta, R. Pizzoferrato, *ChemPhysChem* **2018**, *19*, 2243.
[121] R. Kaur, F. Possanza, F. Limosani, S. Bauroth, R. Zanoni, T. Clark, G. Arrigoni, P. Tagliatesta, D. M. Guldi, *J. Am. Chem. Soc.* **2020**, *142*, 7898.
[122] F. Limosani, R. Kaur, A. Cataldo, S. Bellucci, F. Micciulla, R. Zanoni, A. Lembo, B. Wang, R. Pizzoferrato, D. M. Guldi, P. Tagliatesta, *Angew. Chem., Int. Ed.* **2020**, *59*, 2.
[123] J. Düring, A. Kunzmann, M. S. Kilian, R. D. Costa, D. M. Guldi, F. Gröhn, *ChemPhotoChem* **2018**, *2*, 213.
[124] A. Burger, A. Kunzmann, R. D. Costa, R. Srikantharajah, W. Peukert, D. M. Guldi, A. Hirsch, *Chem. - Eur. J.* **2018**, *24*, 7896.
[125] V. Nikolaou, G. Charalambidis, K. Ladomenou, E. Nikoloudakis, C. Drivas, I. Vamvasakis, S. Panagiotakis, G. Landrou, E. Agapaki, C. Stangel, C. Henkel, J. Joseph, G. Armatas, M. Vasilopoulou, S. Kennou, D. M. Guldi, A. G. Coutsolelos, unpublished.
[126] J. L. Blackburn, *ACS Energy Lett.* **2017**, *2*, 1598.
[127] L. M. Arellano, H. B. Gobeze, M. J. G. Escalonilla, J. L. G. Fierro, F. D'Souza, F. Langa, *Nanoscale* **2020**, *12*, 9890.
[128] L. Dai, D. W. Chang, J. -B. Baek, W. Lu, *Small* **2012**, *8*, 1130.
[129] T. Miletic, E. Pavoni, V. Trifiletti, A. Rizzo, A. Listorti, S. Colella, N. Armaroli, D. Bonifazi, *ACS Appl. Mater. Interfaces* **2016**, *8*, 27966.
[130] J. T. Margraf, F. Lodermeyer, V. Strauss, P. Haines, J. Walter, W. Peukert, R. D. Costa, T. Clark, D. M. Guldi, *Nanoscale Horiz.* **2016**, *1*, 220.
[131] D. Kiessling, R. D. Costa, G. Katsukis, J. Malig, F. Lodermeyer, S. Feihl, A. Roth, L. Wibmer, M. Kehrer, M. Volland, P. Wagner, G. G. Wallace, D. L. Officer, D. M. Guldi, *Chem. Sci.* **2013**, *4*, 3085.
[132] M. Volland, A. Lennert, A. Roth, M. Ince, T. Torres, D. M. Guldi, *Nanoscale* **2019**, *11*, 10709.
[133] J. Jiménez-López, B. M. D. Puscher, D. M. Guldi, E. Palomares, *J. Am. Chem. Soc.* **2020**, *142*, 1236.
[134] J.-F. Eckert, J.-F. Nicoud, J.-F. Nierengarten, S.-G. Liu, L. Echegoyen, F. Barigelletti, N. Armaroli, L. Ouali, V. Krasnikov, G. Hadziioannou, *J. Am. Chem. Soc.* **2000**, *122*, 7467.
[135] L. Jia, M. Chen, S. Yang, *Mater. Chem. Front.* **2020**, *4*, 2256.
[136] L. F. Dössel, V. Kamm, I. A. Howard, F. Laquai, W. Pisula, X. Feng, C. Li, M. Takase, T. Kudernac, S. De Feyter, K. Müllen, *J. Am. Chem. Soc.* **2012**, *134*, 5876.
[137] R. Soltani, B. M. D. Puscher, A. A. Katbab, I. Levchuk, N. Kazerouni, N. Gasparini, N. Camaioni, A. Osvet, M. Batentschuk, R. H. Fink, D. M. Guldi, T. Ameri, *Phys. Chem. Chem. Phys.* **2018**, *20*, 23674.
[138] M. Izquierdo, B. Platzer, A. J. Stasyuk, O. A. Satasyuk, A. A. Voityuk, S. Cuesta, M. Solà, D. M. Guldi, N. Martín, *Angew. Chem., Int. Ed.* **2019**, *58*, 6932.
[139] A. Hasanzadeh, A. Khataee, M. Zarei, Y. Zhang, *Sci. Rep.* **2019**, *9*, 13780.
[140] M. Barrejon, H. B. Gobeze, M. J. Gomez-Escalonilla, J. L. G. Fierro, M. Zhang, M. Yudasaka, S. Lijima, F. D'Souza, F. Langa, *Nanoscale* **2016**, *8*, 14716.
[141] T. Wei, O. Martin, M. Chen, S. Yang, F. Hauke, A. Hirsch, *Angew. Chem., Int. Ed.* **2019**, *58*, 8058.
[142] P. Haines, H. Hölzel, R. Kaur, N. Jux, D. M. Guldi, unpublished.
[143] T. Wei, O. Martin, S. Yang, F. Hauke, A. Hirsch, *Angew. Chem., Int. Ed.* **2019**, *58*, 816.
[144] T. Wei, F. Hauke, H. Andreas, *Acc. Chem. Res.* **2019**, *52*, 2037.
[145] T. Scharl, A. Cadranel, N. Martin, D. M. Guldi, unpublished.

Alejandro Cadranel graduated in chemical sciences (2008) and obtained his Ph.D. degree (2012) at the University of Buenos Aires (UBA) in Argentina under the supervision of Luis Baraldo. After a postdoctoral period at the same university, he joined Prof. Guldi's group at the University of Erlangen-Nürnberg in 2015 as a postdoctoral researcher. In 2018 he joined UBA and the faculty of the national research council (CONICET). His research focuses on supramolecular photochemistry of donor-acceptor systems and coordination complexes for photon management and catalysis.

Philipp Haines received both his B.Sc. (2013) and M.Sc. (2015) at the Friedrich-Alexander University of Erlangen-Nuremberg (Germany) and joined the group of Prof. Guldi in 2015 for his doctoral research. During his Ph.D. (2020), he joined the group of Prof. Boris Rybtchinski at the Weizmann Institute in Rehovot (Israel) as a visiting researcher. His research encompasses the investigation of nanographenic structures. The focus lies on the photophysical characterization of Hexa-peri-hexabenzocoronene related structures alone and incorporated with photo- and redox-active chromophores.

Ramandeep Kaur received her B.Sc. degree in Chemistry (2013) from Delhi University, India. In 2013, she moved to Germany where she graduated with an M.Sc. degree in Chemistry (2015) from the Friedrich-Alexander University of Erlangen-Nuremberg, Germany. At this University she joined the research group of Prof. D. M. Guldi in 2015 as a Ph.D. student. Her doctoral research is focused on the investigation of photoinduced charge-transfer process in novel electron donor-acceptor covalent and supramolecular architectures.

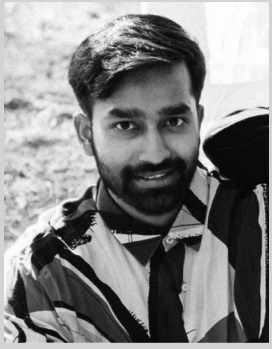

Arjun Menon received his B.Sc. (2010) from Madras Christian College and M.Sc. (2012) from Loyola College, affiliated with the University of Madras (India). After graduation, he has worked as an Executive-Quality Assurance (2013) at TTK. Healthcare. Ltd (India) and Research Associate (2014) at Loyola Institute of Frontier Energy (India). In 2015, he moved to Germany and joined NBHX Trimm GmbH as Production and Quality Controller. Since 2017, he is a Ph.D. student in the research group of Prof. Guldi at Friedrich-Alexander University of Erlangen. His research field is the characterization and electronic fine-tuning of functionalized carbon nanomaterials. He primarily focuses on the non-covalent interactions between SWCNTs as well as photoactive building blocks.

Peter W. Münich received his B.Sc. (2012) and M.Sc. (2014) degree in molecular science from the Friedrich-Alexander University Erlangen-Nuremberg (Germany). He received his doctor's degree (Dr. rer. nat.) (2020) from the Friedrich-Alexander University Erlangen-Nuremberg in the group of Prof. Guldi as a member of the Graduate School Molecular Science. The focus of his ongoing research in the group of Prof. Guldi is the individualization and doping of SWCNTs in supramolecular assemblies with molecular dyes and the resulting intra- and intermolecular interactions.

Peter R. Schol received his B.Sc. (2016) and M.Sc. (2019) from the Friedrich-Alexander-University of Erlangen-Nuremberg (Germany), joining the group of Prof. Guldi in 2019 for his doctoral research. His research field is the optimization and characterization of dye-sensitized solar cells for efficient and sustainable energy generation. He primarily focuses on the characterization and implementation of singlet fission capable dyes into solar cell schemes.

Dirk M. Guldi completed both his undergraduate studies (1988) and Ph.D. (1990) at the University of Cologne (Germany). Following postdoctoral appointments at the National Institute of Standards and Technology (USA), the Hahn-Meitner Institute Berlin (1992), and Syracuse University, he joined the faculty of the Notre Dame Radiation Laboratory in 1995. He was promoted a year later from assistant to associate professional specialist, and remained affiliated to Notre Dame until 2004. Since 2004, he is Full Professor in the Department of Chemistry and Pharmacy at the Friedrich-Alexander University in Erlangen.